Cell Reports

Article

Identification and functional validation of FDA-approved positive and negative modulators of the mitochondrial calcium uniporter

Graphical abstract

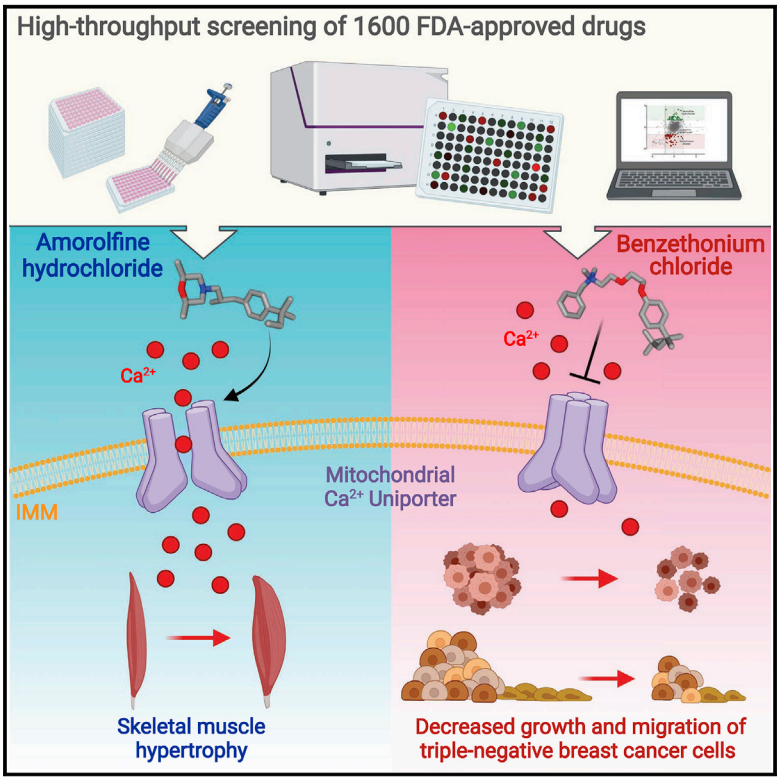

Highlights

- We screen an FDA-approved drug library for mitochondrial Ca^{2+} uptake modulators
- Amorolfine and benzethonium modulate MCU activity
- Amorolfine increases MCU-dependent mitochondrial metabolism and muscle size
- Benzethonium decreases MCU-dependent cancer cell growth and migration

Authors

Agnese De Mario, Anna Tosatto, Julia Marie Hill, ..., Gyorgy Szabadkai, Rosario Rizzuto, Cristina Mammucari

Correspondence

rosario.rizzuto@unipd.it (R.R.), cristina.mammucari@unipd.it (C.M.)

In brief

In search of mitochondrial Ca^{2+} uptake modulators, De Mario et al. identify amorolfine and benzethonium as positive hits of a 1,600 FDA drug library high-throughput screen. Amorolfine increases mitochondrial metabolism and muscle size in an MCU-dependent manner. Benzethonium negatively regulates MCU activity, mROS formation, and cancer cell growth and migration.

De Mario et al., 2021, Cell Reports *35*, 109275
June 22, 2021
https://doi.org/10.1016/j.celrep.2021.109275

CellPress

Cell Reports

CellPress
OPEN ACCESS

Article

Identification and functional validation of FDA-approved positive and negative modulators of the mitochondrial calcium uniporter

Agnese De Mario,[1] Anna Tosatto,[1] Julia Marie Hill,[2,8] Janos Kriston-Vizi,[3] Robin Ketteler,[4] Denis Vecellio Reane,[1] Gino Cortopassi,[5] Gyorgy Szabadkai,[1,2,6] Rosario Rizzuto,[1,7,*] and Cristina Mammucari[1,7,9,*]

[1]Department of Biomedical Sciences, University of Padua, 35131 Padua, Italy
[2]Department of Cell and Developmental Biology, Consortium for Mitochondrial Research, University College London, London WC1E 6BT, UK
[3]Bioinformatics Image Core (BIONIC), MRC Laboratory for Molecular Cell Biology, University College London, Gower Street, London WC1E 6BT, UK
[4]Cell Signalling and Autophagy Group, MRC Laboratory for Molecular Cell Biology, University College London, Gower Street, London WC1E 6BT, UK
[5]Department of Molecular Bioscience, School of Veterinary Medicine, University of California, Davis, Davis, CA 95616, USA
[6]Francis Crick Institute, London WC1E 6BT, UK
[7]Myology Center (CIR-Myo), University of Padua, 35131 Padua, Italy
[8]Present address: International Collaboration on Repair Discoveries (ICORD), University of British Columbia, Vancouver, BC, Canada
[9]Lead contact
*Correspondence: rosario.rizzuto@unipd.it (R.R.), cristina.mammucari@unipd.it (C.M.)
https://doi.org/10.1016/j.celrep.2021.109275

SUMMARY

The mitochondrial calcium uniporter (MCU), the highly selective channel responsible for mitochondrial Ca^{2+} entry, plays important roles in physiology and pathology. However, only few pharmacological compounds directly and selectively modulate its activity. Here, we perform high-throughput screening on a US Food and Drug Administration (FDA)-approved drug library comprising 1,600 compounds to identify molecules modulating mitochondrial Ca^{2+} uptake. We find amorolfine and benzethonium to be positive and negative MCU modulators, respectively. In agreement with the positive effect of MCU in muscle trophism, amorolfine increases muscle size, and MCU silencing is sufficient to blunt amorolfine-induced hypertrophy. Conversely, in the triple-negative breast cancer cell line MDA-MB-231, benzethonium delays cell growth and migration in an MCU-dependent manner and protects from ceramide-induced apoptosis, in line with the role of mitochondrial Ca^{2+} uptake in cancer progression. Overall, we identify amorolfine and benzethonium as effective MCU-targeting drugs applicable to a wide array of experimental and disease conditions.

INTRODUCTION

Mitochondrial Ca^{2+} uptake buffers cytosolic Ca^{2+}, regulates signal transduction, modulates bioenergetics, and controls cell death pathways. Ca^{2+} rapidly enters the mitochondrial matrix by virtue of an electrogenic mechanism driven by the large voltage generated across the inner mitochondrial membrane (IMM). Mitochondrial Ca^{2+} uptake relies on the activity of a highly selective channel, the mitochondrial calcium uniporter (MCU) (Baughman et al., 2011; De Stefani et al., 2011). Although mitochondrial Ca^{2+} uptake is limited at resting cytosolic [Ca^{2+}], it rises rapidly when [Ca^{2+}] in close proximity to mitochondria reaches a threshold value. This is due to the close proximity of mitochondria to the main intracellular Ca^{2+} store, the endoplasmic reticulum (ER). Upon physiological stimuli that trigger ER Ca^{2+} release, microdomains of high [Ca^{2+}] are formed at ER-mitochondria contacts, allowing MCU opening (Rizzuto et al., 2012). Regulatory subunits participate in this gatekeeping mechanism. In particular, MICU1 and MICU2, two MCU interactors of the inter-membrane space, form a heterodimer that senses cytosolic [Ca^{2+}] and tunes MCU activity (Csordás et al., 2013; Mallilankaraman et al., 2012; Patron et al., 2014).

Efforts have been made to identify small molecules to inhibit MCU activity. The thiourea KB-R7943, initially developed as a negative modulator of the plasma membrane Na^+/Ca^{2+} exchanger, also inhibits the MCU, resulting in cardiac protection from ischemia-reperfusion (I/R) injury (Santo-Domingo et al., 2007). Another compound, Ru265, is a synthetic derivative of the widely used Ru360 (Ying et al., 1991; Matlib et al., 1998; Emerson et al., 1993). Compared with the cell-impermeable Ru360, Ru265 targets the MCU in intact cells and inhibits mitochondrial Ca^{2+} uptake with enhanced efficacy. Ru265 prevents mitochondrial swelling and mitochondrial membrane potential dissipation in I/R injury (Woods et al., 2019). By screening small-molecule libraries, other cell-permeable inhibitors of mitochondrial Ca^{2+} uptake were identified, including DS16570511, which, in isolated hearts, prevents mitochondrial Ca^{2+} overload and increases contractility (Kon et al., 2017). An innovative

method based on yeast bioenergetics shunting was introduced to minimize the false discovery rate of MCU inhibitors because of compounds affecting mitochondrial bioenergetics and membrane potential. By screening a library of 600 clinically approved compounds, the antineoplastic drug mitoxantrone was identified as a selective MCU inhibitor. The side arms of mitoxantrone are required for MCU inhibition, whereas the quinizarin moiety, necessary for intercalation into DNA and inhibition of topoisomerase II, is dispensable (Arduino et al., 2017). Recently, MCU-i4 and MCU-i11 were identified as small molecules able to decrease mitochondrial Ca^{2+} uptake in a MICU1-dependent manner in cell lines and in adult myofibers (Di Marco et al., 2020). Regarding positive MCU modulators, the p38 mitogen-activated protein kinase inhibitor SB202190 modulates mitochondrial Ca^{2+} with a mechanism independent of p38 activity (Montero et al., 2002). In addition, several natural plant flavonoids have been shown to increase MCU activity independent of their antioxidant activity (Montero et al., 2004). Finally, agonists and antagonists of the estrogen receptor modulate the activity of the uniporter. In particular, 4,4′,4″-(4-propyl-[1 h]-pyrazole-1,3,5-triyl)trisphenol (PPT), diethylstilbestrol, and 17-β-estradiol activate mitochondrial Ca^{2+} uptake, whereas tamoxifen and 4-hydroxy-tamoxifen inhibit it (Lobatón et al., 2005).

In search of compounds that modulate MCU activity, we screened a library comprising 1,600 US Food and Drug Administration (FDA)-approved drugs for their ability to act on mitochondrial Ca^{2+} uptake without impinging on cytosolic Ca^{2+} transients. False positive hits, including drugs that dissipate the $\Delta\Psi_m$ or that are ineffective in increasing mitochondrial Ca^{2+} uptake speed in permeabilized cells, were excluded. We identified amorolfine and benzethonium as an activator and inhibitor of mitochondrial Ca^{2+} uptake, respectively.

Amorolfine is a morpholine antifungal drug that inhibits the fungal sterol synthesis pathway, and it is indicated for topic treatment of mycoses. In agreement with the role of MCU in triggering hypertrophy (Mammucari et al., 2015), amorolfine increased myotube size *in vitro* in an MCU-dependent manner and triggered muscle hypertrophy *in vivo*.

Benzethonium is a synthetic quaternary ammonium salt with antiseptic properties. The negative effects of benzethonium on mitochondrial Ca^{2+} uptake were verified in MDA-MB-231 cells, a triple-negative breast cancer cell line in which, similar to MCU silencing (Tosatto et al., 2016), drug treatment decreased cell migration and growth. In addition, in line with the role of mitochondrial Ca^{2+} uptake in cell death (Rizzuto et al., 2012), benzethonium increased cell survival upon pro-apoptotic stimuli.

Thus, amorolfine and benzethonium represent leading, clinically approved drugs able to impinge on mitochondrial Ca^{2+} uptake in different pathophysiological settings.

RESULTS

High-throughput screening identifies FDA-approved MCU modulators

In search of clinically approved drugs that modulate mitochondrial Ca^{2+} uptake, we designed a high-throughput screening approach using the Ca^{2+}-sensitive recombinant photoprotein aequorin targeted to the mitochondrial matrix (mitAEQ) and to the cytoplasm (cytAEQ) (Tosatto et al., 2017). This approach allowed us to identify small compounds in an FDA-approved drug library (MicroSource Pharmakon-1600) that specifically modulate mitochondrial Ca^{2+} uptake with minimal interference with upstream cytosolic Ca^{2+} signals. HeLa cells were transfected with plasmids encoding mitAEQ or cytAEQ and reconstituted with the prosthetic group coelenterazine. Ca^{2+} release from ER stores was triggered by inositol 1,4,5-trisphosphate (IP_3) using histamine as a Ca^{2+}-mobilizing stimulus, and the subsequent increases in mitochondrial and cytosolic [Ca^{2+}] were measured.

To assess the effect of individual compounds on mitochondrial Ca^{2+} signals, cells were treated for 30 min with 1,600 compounds prior to Ca^{2+} measurements. Mitochondrion-specific hits were defined as compounds (1) modulating the peak mitochondrial Ca^{2+} signal in the positive or negative direction (Z score greater than −1.645 or less than 1.645, 5th percentile) and (2) not affecting the peak cytosolic Ca^{2+} signal by more than 2.054 Z scores across all samples (Z score greater than −2.054 and less than 2.054, second percentile) (Figure 1A; Table S1). The screen resulted in 66 inhibitor and 54 activator hits of mitochondrial Ca^{2+} uptake. The hits were further prioritized based on their chemical properties, known functions, and effect on mitochondrial membrane potential ($\Delta\Psi_m$). We searched for compounds acting directly on the Ca^{2+} uptake machinery directly and, thus, excluded compounds that modulate Ca^{2+} uptake indirectly by altering $\Delta\Psi_m$. Based on these considerations, we further analyzed three compounds: amorolfine, duloxetine, and benzethonium (Figure 1B).

Amorolfine is a positive MCU modulator

High-throughput screening identified the morfoline-derivative drug amorolfine as a strong positive modulator of mitochondrial Ca^{2+} uptake. We verified this result in a small-scale perfusion system that allows discerning the rapid effects of plasma-membrane receptor activation on Ca^{2+} transients from long-term responses because of alternative mechanisms. We first measured Ca^{2+} transients upon histamine stimulation in HeLa cells treated acutely with 10 μM amorolfine. Similar to the high-throughput screening results, amorolfine increased mitochondrial Ca^{2+} uptake (Figures 2A and S1A) without affecting cytosolic Ca^{2+} transients (Figure 2B). The half-maximal effective concentration (EC_{50}) was 86.88 × 10^{-6} M. We next tested whether this effect was specific to histamine receptors. We triggered intracellular Ca^{2+} mobilization by IP_3 generated in response to purinergic receptors activation. Cells were stimulated with ATP, and Ca^{2+} transients were measured upon acute amorolfine treatment. Similarly to what was observed after histamine treatment, amorolfine triggered a 2-fold increase in ATP-induced mitochondrial Ca^{2+} uptake (Figure 2C) without affecting cytosolic Ca^{2+} transients (Figure 2D). These data indicate that amorolfine increases mitochondrial Ca^{2+} uptake independent of the Ca^{2+} transient trigger, suggesting that the drug specifically modulates the activity of the MCU. To verify this hypothesis, we measured mitochondrial Ca^{2+} uptake speed in permeabilized cells, in which intracellular Ca^{2+} stores are depleted and mitochondria are exposed to a buffer containing a well-defined [Ca^{2+}]. Under these experimental conditions, amorolfine was able to increase mitochondrial Ca^{2+} uptake speed (Figure 2E), demonstrating

A

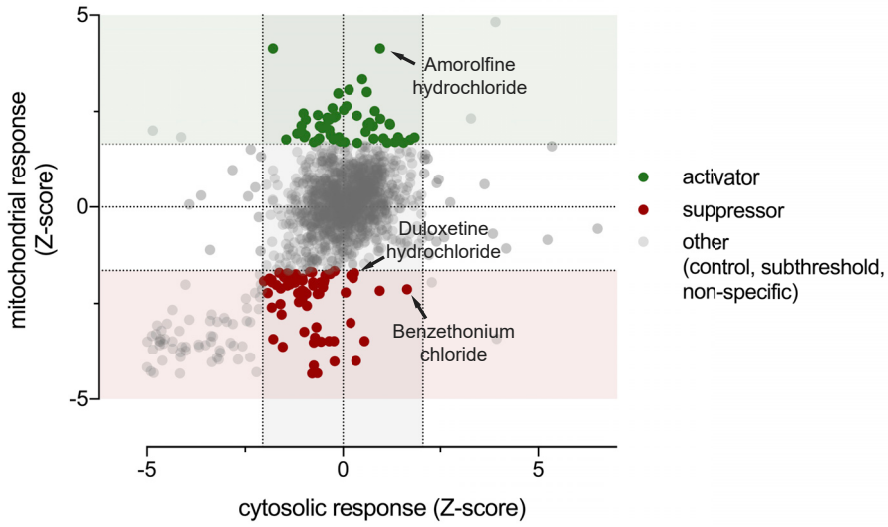

B

Name	Structure	IUPAC name
Amorolfine hydrochloride	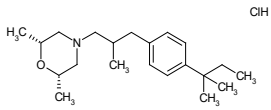	(2R,6S)-2,6-dimethyl-4-[2-methyl-3-[4-(2-methylbutan-2-yl)phenyl]propyl]morpholine;hydrochloride
Benzethonium chloride	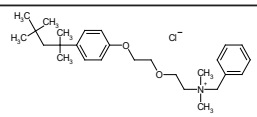	benzyl-dimethyl-[2-[2-[4-(2,4,4-trimethylpentan-2-yl)phenoxy]ethoxy]ethyl]azanium;chloride
Duloxetine hydrochloride	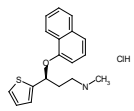	(3S)-N-methyl-3-naphthalen-1-yloxy-3-thiophen-2-ylpropan-1-amine;hydrochloride

Figure 1. A high-throughput screening identified MCU modulators

(A) Distribution of *Z* scores calculated for mitochondrial and cytosolic Ca^{2+} transients for each analyzed drug. A *Z* score limit to identify positive and negative modulators of mitochondrial Ca^{2+} uptake was applied (colored zones, 5th percentile for mitochondrial Ca^{2+} and more stringent second percentile for cytosolic Ca^{2+} responses). Activators have a mitochondrial *Z* score greater than 1.645 and cytosolic *Z* score greater than −2.054 and less than 2.054. Suppressors have a mitochondrial *Z* score of less than −1.645 and cytosolic *Z* score greater than −2.054 and less than 2.054.

(B) Names and chemical structures of selected drugs.

that the drug directly increases MCU activity. Amorolfine also increased mitochondrial Ca^{2+} uptake in permeabilized cells in a different experimental setup, based on comparison of extramitochondrial Ca^{2+} removal rates before and after drug treatment in the same cell population (Figure 2F). The effects of amorolfine on mitochondrial Ca^{2+} uptake were not due to differences in $\Delta\Psi_m$, which remained unaltered in amorolfine-treated cells (Figure S1B). Upon 24 h of incubation, amorolfine did not affect cell viability (Figure S1C). Thus, amorolfine is a *bona fide* MCU activator.

Amorolfine triggers MCU-dependent skeletal muscle hypertrophy

Loss-of-function mutations in the MICU1 gene are responsible for impaired mitochondrial Ca^{2+} signaling and diseases affecting the nervous system and musculature with symptoms that include muscle weakness, ataxia, and fatigue (Logan et al., 2014; Lewis-Smith et al., 2016; Musa et al., 2018). The muscle phenotype of skeletal muscle-specific *MICU1*$^{-/-}$ mice is similar to the clinical manifestations, demonstrating that a primary defect in skeletal muscle Ca^{2+} handling underlies the disease (Debattisti et al., 2019). We reported previously that pharmacological targeting of MICU1-dependent mitochondrial Ca^{2+} uptake (Di Marco et al., 2020) and genetic targeting of the MCU (Mammucari et al., 2015; Gherardi et al., 2019) reduce muscle size. MCU overexpression triggers muscle hypertrophy (Mammucari et al., 2015). Thus, we wanted to find out whether amorolfine, by increasing MCU activity, would increase muscle size.

First we checked the effect of acute amorolfine treatment on agonist-induced mitochondrial Ca^{2+} uptake and cytosolic Ca^{2+} transients in C2C12 myoblasts. Compared with control cells, treatment with 0.1 μM amorolfine was sufficient to trigger an

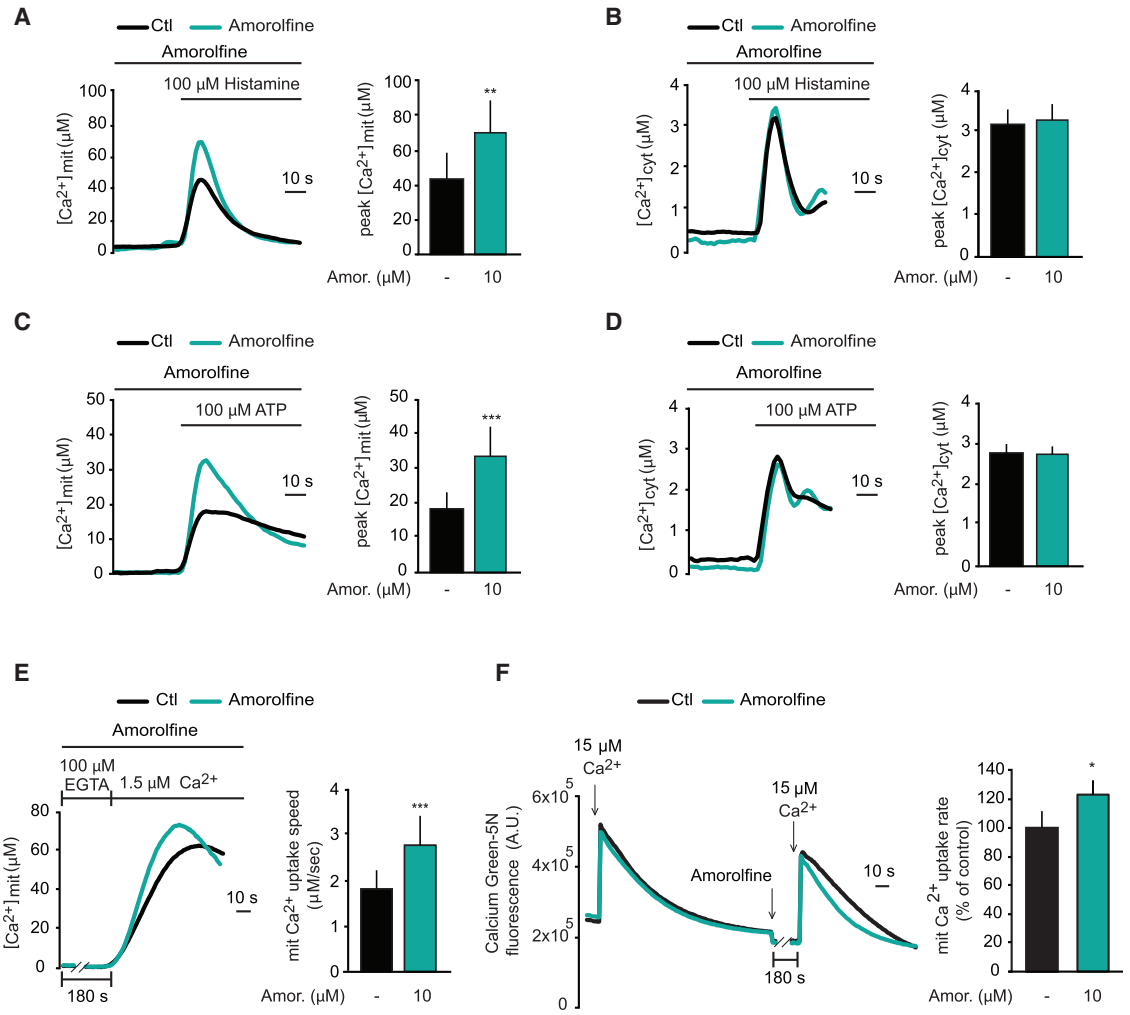

Figure 2. Amorolfine is a positive MCU modulator

(A) Agonist-induced mitochondrial Ca^{2+} uptake in intact HeLa cells. Cells were treated with amorolfine or DMSO before (30 s) and during histamine stimulation. Left: representative traces. Right: mean $[Ca^{2+}]_{mit}$ peaks.

(B) Agonist-induced cytosolic Ca^{2+} transients in intact HeLa cells. Cells were treated with amorolfine or DMSO before (30 s) and during histamine stimulation. Left: representative traces. Right: mean $[Ca^{2+}]_{cyt}$ peaks.

(C) Agonist-induced mitochondrial Ca^{2+} uptake in intact HeLa cells. Cells were treated with amorolfine or DMSO before (30 s) and during ATP stimulation. Left: representative traces. Right: mean $[Ca^{2+}]_{mit}$ peaks.

(D) Agonist-induced cytosolic Ca^{2+} transients in intact HeLa cells. Cells were treated with amorolfine or DMSO before (30 s) and during ATP stimulation. Left: representative traces. Right: mean $[Ca^{2+}]_{cyt}$ peaks.

(E) Mitochondrial Ca^{2+} uptake measurements in permeabilized HeLa cells. Cells were treated with amorolfine or DMSO before (180 s) and during Ca^{2+} perfusion. Left: representative traces. Right: mean $[Ca^{2+}]_{mit}$ speed.

(F) Extramitochondrial Ca^{2+} removal in permeabilized HeLa cells, measured by Calcium Green-5N fluorescence. After addition of a first bolus of $CaCl_2$, amorolfine or DMSO was added. 3 min later, a second bolus of $CaCl_2$ was added. For each sample, the ratio of the two mitochondrial Ca^{2+} uptake rates was calculated. Left: representative traces. Right: percentage of vehicle ratio (control).

Data are presented as mean ± SD. *p < 0.05, **p < 0.01, ***p < 0.001; Student's two-tailed t test except Mann-Whitney rank-sum test for (B).

~2-fold increase in mitochondrial Ca^{2+} uptake (Figure 3A). According to the stronger effect compared with HeLa cells, the EC_{50} of amorolfine in C2C12 myoblasts was 8.1×10^{-8} M. Amorolfine did not impinge on cytosolic $[Ca^{2+}]$ transients (Figure 3B). Resting mitochondrial and cytosolic $[Ca^{2+}]$ were unaltered, too (Figures S2A and S2B). After having assessed that amorolfine does not affect C2C12 myoblast viability (Figure S2C), we explored the role of the drug in myotube growth. C2C12 myoblasts were cultured in a differentiating medium in the presence or absence of amorolfine, and myotube size was measured (Figure 3C). Drug treatment was sufficient to trigger a significant increase in myotube size compared with untreated cells (Figures 3D–3F). Amorolfine reduced the mRNA expression of myoblast proliferation markers, including MyoD and Myf5 (Figures S2D and S2E). These data suggest that amorolfine promotes C2C12 differentiation and myotube growth.

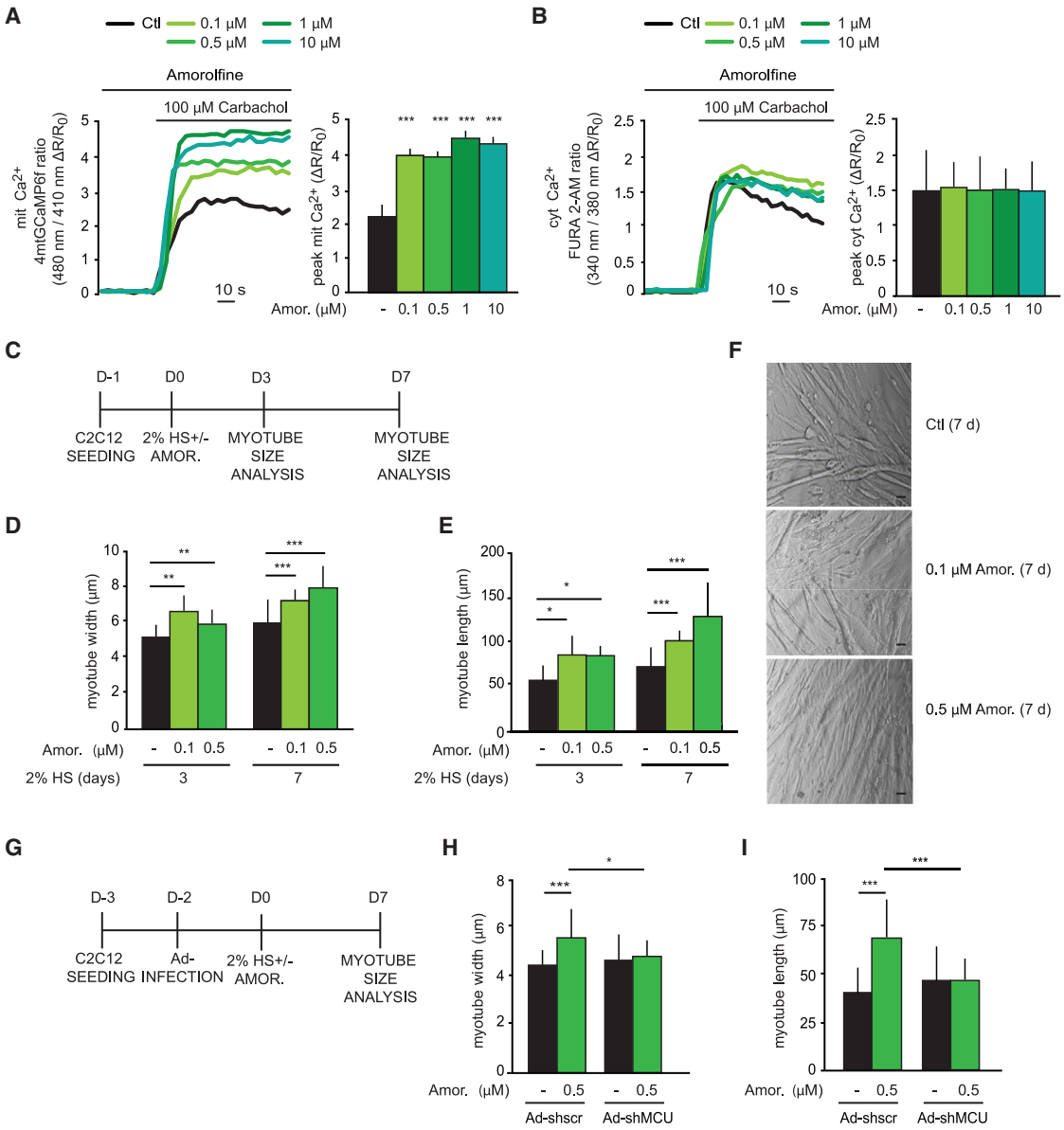

Figure 3. Amorolfine increases C2C12 myotube size in an MCU-dependent manner

(A) Agonist-induced mitochondrial Ca^{2+} uptake in C2C12 myoblasts. Cells were treated with amorolfine or DMSO before (30 s) and during carbachol stimulation. Left: representative traces. Right: mean $[Ca^{2+}]_{mit}$ peaks.

(B) Agonist-induced cytosolic Ca^{2+} transients in C2C12 myoblasts. Cells were treated with amorolfine or DMSO before (30 s) and during carbachol stimulation. Left: representative traces. Right: mean $[Ca^{2+}]_{cyt}$ peaks.

(C) Representative scheme of the experimental design. The day after C2C12 myoblast seeding, growth medium was replaced with 2% horse serum (HS)-containing medium to induce cell differentiation, and amorolfine treatment was performed. Myotube width and length were measured at the indicated time points.

(D) Measurements of C2C12 myotube width upon amorolfine treatment as depicted in (C).

(E) Measurements of C2C12 myotube length upon amorolfine treatment as depicted in (C).

(F) Representative images of C2C12 myotubes treated with amorolfine or DMSO as control (Ctl) as depicted in (C). Scale bar, 5 µm.

(G) Representative scheme of the experimental design. The day after C2C12 myoblast seeding, cells were infected with Ad-shMCU or a control virus expressing a scrambled short hairpin RNA (Ad-shscr). Two days later, growth medium was replaced with 2% HS-containing medium to induce myotube formation, and amorolfine treatment was performed. Myotube width and length were measured at the indicated time points.

(H) Measurements of C2C12 myotube width upon MCU silencing and amorolfine treatment ad depicted in (G).

(I) Measurements of C2C12 myotube length upon MCU silencing and amorolfine treatment as depicted in (G).

Data are presented as mean ± SD. *p < 0.05, **p < 0.01, ***p < 0.001; two-way ANOVA except one-way ANOVA for (A) and (B).

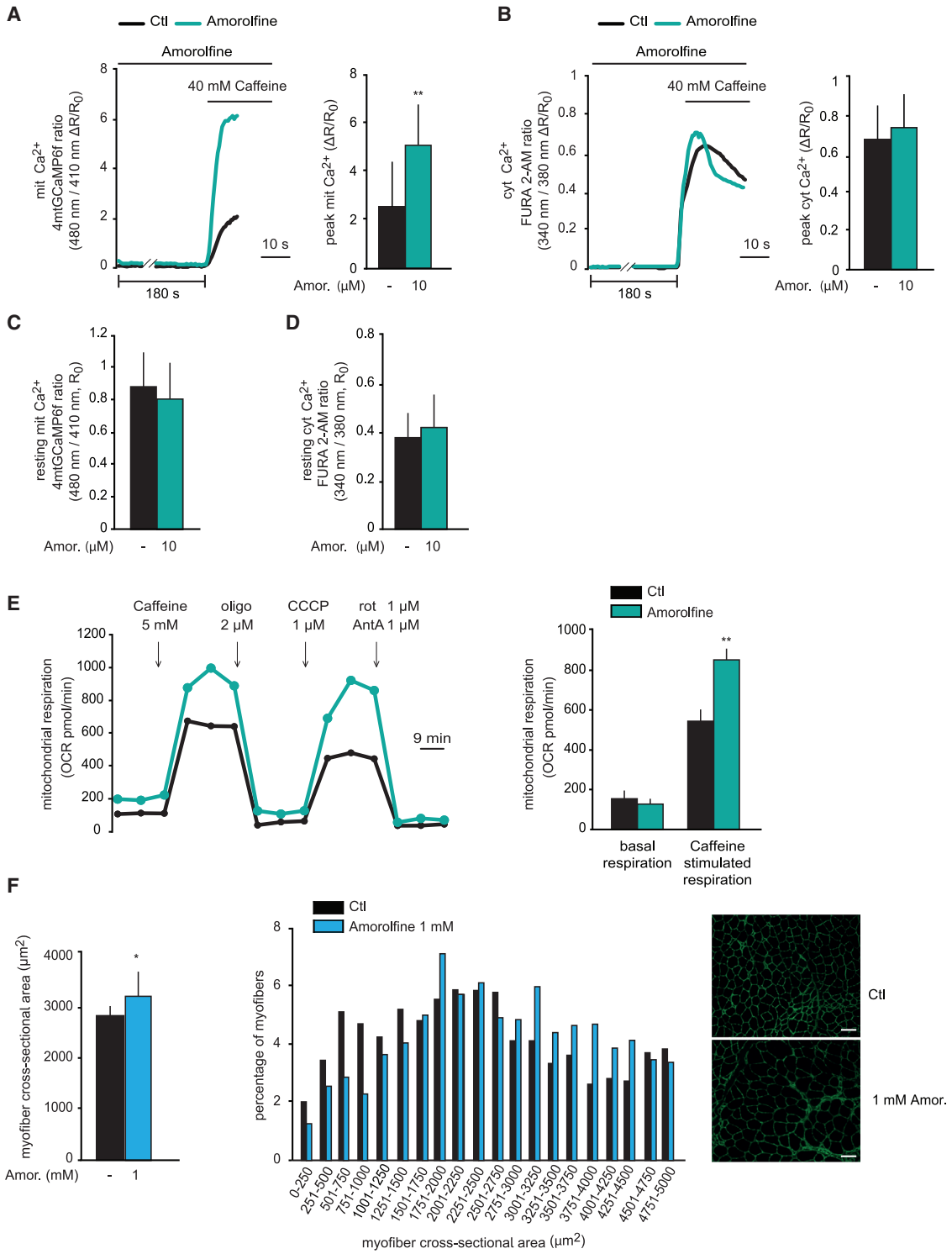

Figure 4. Amorolfine induces skeletal muscle hypertrophy *in vivo*

(A) Agonist-induced mitochondrial Ca^{2+} uptake in adult myofibers of *flexor digitorum brevis* (FDB) muscles. FDB muscles were transfected *in vivo* with the mitochondrial Ca^{2+} probe 4mtGCaMP6f. 7 days later, isolated myofibers were treated with amorolfine or DMSO before (180 s) and during caffeine stimulation. Left: representative traces. Right: mean $[Ca^{2+}]_{mit}$ peaks.

(B) Agonist-induced cytosolic Ca^{2+} transients in FDB adult myofibers. Isolated myofibers were loaded with fura-2-acetoxymethyl ester (FURA-2 AM). 20 min later, they were treated with amorolfine or DMSO before (180 s) and during caffeine stimulation. Left: representative traces. Right: mean $[Ca^{2+}]_{cyt}$ peaks.

(legend continued on next page)

To verify the hypothesis that amorolfine increases the size of C2C12 myotubes by positively modulating mitochondrial Ca^{2+} entry, we tested whether the MCU was required for drug-induced myotube growth. We infected C2C12 myoblasts with an adenoviral vector expressing a short-hairpin RNA against MCU (Ad-shMCU). Two days later, we replaced the growth medium with differentiating medium in the presence or absence of amorolfine. Seven days after induction of differentiation, when MCU protein levels were reduced significantly (Figure S2F), we performed myotube size measurements (Figure 3G). MCU silencing abrogated the increase in C2C12 size induced by amorolfine, demonstrating that mitochondrial Ca^{2+} uptake is required (Figures 3H and 3I). Although MCU silencing or deletion per se triggered atrophy *in vivo* (Mammucari et al., 2015; Gherardi et al., 2019), it did not affect C2C12 myotube formation *in vitro*. This may be due to the different structural and functional properties of C2C12 cells compared with animal muscle, including lack of excitation-contraction (EC) coupling and differences in mitochondrial positioning and mitochondrial contacts with the sarcoplasmic reticulum (SR) and the plasma membrane. Thus, in adult muscle, mitochondrial Ca^{2+} homeostasis would decode multiple signals that are dispensable in C2C12 cell culture.

Next we tested whether amorolfine had similar effects *ex vivo* and *in vivo*. We measured mitochondrial Ca^{2+} uptake and cytosolic Ca^{2+} transients in *flexor digitorum brevis* (FDB) muscle fibers freshly isolated from adult mice and treated with the drug or left untreated. In line with data obtained in cell lines, amorolfine increased caffeine-induced mitochondrial Ca^{2+} uptake in myofibers (Figure 4A) without affecting cytosolic Ca^{2+} transients (Figure 4B). Moreover, amorolfine did not alter resting mitochondrial and cytosolic Ca^{2+} levels (Figures 4C and 4D). In light of the role of mitochondrial Ca^{2+} uptake to stimulate tricarboxylic acid (TCA) cycle activity, we evaluated whether amorolfine triggered an increase in the oxygen consumption rate (OCR) of adult mouse myofibers. Although basal respiration was unaffected, the increase in OCR triggered by caffeine-induced SR Ca^{2+} release was greater in amorolfine-treated myofibers compared with control counterparts (Figure 4E).

Finally, we validated the *in vivo* effects of amorolfine on muscle size. Administered locally by intramuscular injection, amorolfine significantly increased the cross-sectional area of *tibialis anterior* (TA) muscle fibers (Figure 4F), demonstrating that a trophic effect can be achieved by pharmacological modulation of the MCU.

Duloxetine exerts multiple effects on Ca^{2+} homeostasis

Ca^{2+} entry into the mitochondrial matrix is driven by the large $\Delta\Psi_m$ generated across the IMM. Although collapse of the $\Delta\Psi_m$ causes a sudden drop in agonist-induced mitochondrial Ca^{2+} uptake, genuine MCU inhibitors decrease mitochondrial Ca^{2+} uptake in energized mitochondria. Thus, to identify false positive inhibitors of the MCU, we measured $\Delta\Psi_m$ in HeLa cells upon treatment with drugs selected from high-throughput screening. Drugs that dissipated the $\Delta\Psi_m$ were excluded from further analysis (data not shown). We then focused on two drugs (benzethonium and duloxetine) identified by high-throughput screening as negative modulators of mitochondrial Ca^{2+} uptake when IP_3 generation was triggered by histamine stimulation and confirmed not to alter the $\Delta\Psi_m$ (Figures 5A and S3A).

We further analyzed the effects of duloxetine on Ca^{2+} homeostasis. In permeabilized cells, duloxetine decreased the speed of mitochondrial Ca^{2+} entry, indicating a direct effect on the MCU (Figure S3B). In addition, aequorin-based measurements in intact cells perfused acutely with duloxetine confirmed the negative effect of the drug on histamine-induced mitochondrial Ca^{2+} transients (Figure S3C). However, although the high-throughput screening detected negligible effects of duloxetine on cytosolic Ca^{2+} transients, the perfusion system uncovered negative modulation of cytosolic [Ca^{2+}] upon histamine stimulation (Figure S3D), suggesting that the drug affects global Ca^{2+} homeostasis. To verify whether, in addition to a direct effect on the MCU, duloxetine impinges on plasma-membrane receptors upstream of the IP_3-generating machinery, we measured the effects of the drug on mitochondrial Ca^{2+} uptake in cells treated with the purinergic receptor agonist ATP. Contrary to histamine-stimulated cells, duloxetine increased mitochondrial Ca^{2+} uptake and cytosolic Ca^{2+} transients in ATP-treated cells (Figures S3E and S3F), suggesting that this drug has multiple targets, impinging on the MCU and on cell-membrane receptors linked to IP_3 generation. Moreover, in the latter case, it exerts opposite effects on histamine and on purinergic receptors, indicating complex activity. In accordance with our scope (i.e., identify specific MCU modulators), we did not pursue analysis of this drug.

Benzethonium is a negative MCU modulator

We then performed similar analyses on benzethonium. As reported above, benzethonium did not affect $\Delta\Psi_m$ (Figure 5A). In permeabilized cells, it blunted mitochondrial Ca^{2+} uptake speed (Figure 5B) and had a negative effect in experiments in which the rates of extra-mitochondrial Ca^{2+} removal were compared before and after drug addition (Figure 5C).

Surprisingly, when perfused acutely on intact cells, the drug did not affect mitochondrial Ca^{2+} uptake (Figure 5D), suggesting that its cell permeability is limited. However, in line with the results of the high-throughput screening, benzethonium strongly reduced histamine-induced mitochondrial Ca^{2+} uptake in cells pre-treated for 1 h with the drug (Figure 5E), with an EC_{50} of

(C) Resting mitochondrial Ca^{2+} levels of single isolated FDB myofibers. FDB muscles were transfected *in vivo* with the mitochondrial Ca^{2+} probe 4mtGCaMP6f. 7 days later, isolated myofibers were treated (180 s) with amorolfine or DMSO and resting mitochondrial Ca^{2+} was measured.
(D) Resting cytosolic Ca^{2+} levels of single isolated FDB myofibers. Isolated myofibers were loaded with FURA-2 AM. 20 min later, they were treated (180 s) with amorolfine or DMSO and resting cytosolic Ca^{2+} was measured.
(E) OCR measurement in isolated FDB myofibers. After isolation, FDB myofibers were treated with amorolfine or DMSO, and 1 h later OCR was measured. To calculate basal and caffeine-induced respiration, non-mitochondrial O_2 consumption was subtracted from absolute values. Data were normalized on mean calcein fluorescence. Left: representative traces. Right: OCR quantification.
(F) Myofiber cross-sectional area of *tibialis anterior* (TA) muscles injected with amorolfine. TA muscles were injected with amorolfine or DMSO every 48 h for 10 days. Left: mean myofiber cross-sectional area. Center: distribution of myofiber cross-sectional area. Right: representative images. Scale bar, 100 μm.
Data are presented as mean ± SD. *$p < 0.05$, **$p < 0.01$; Mann-Whitney rank-sum test except Student's two-tailed t test for (E) and (F).

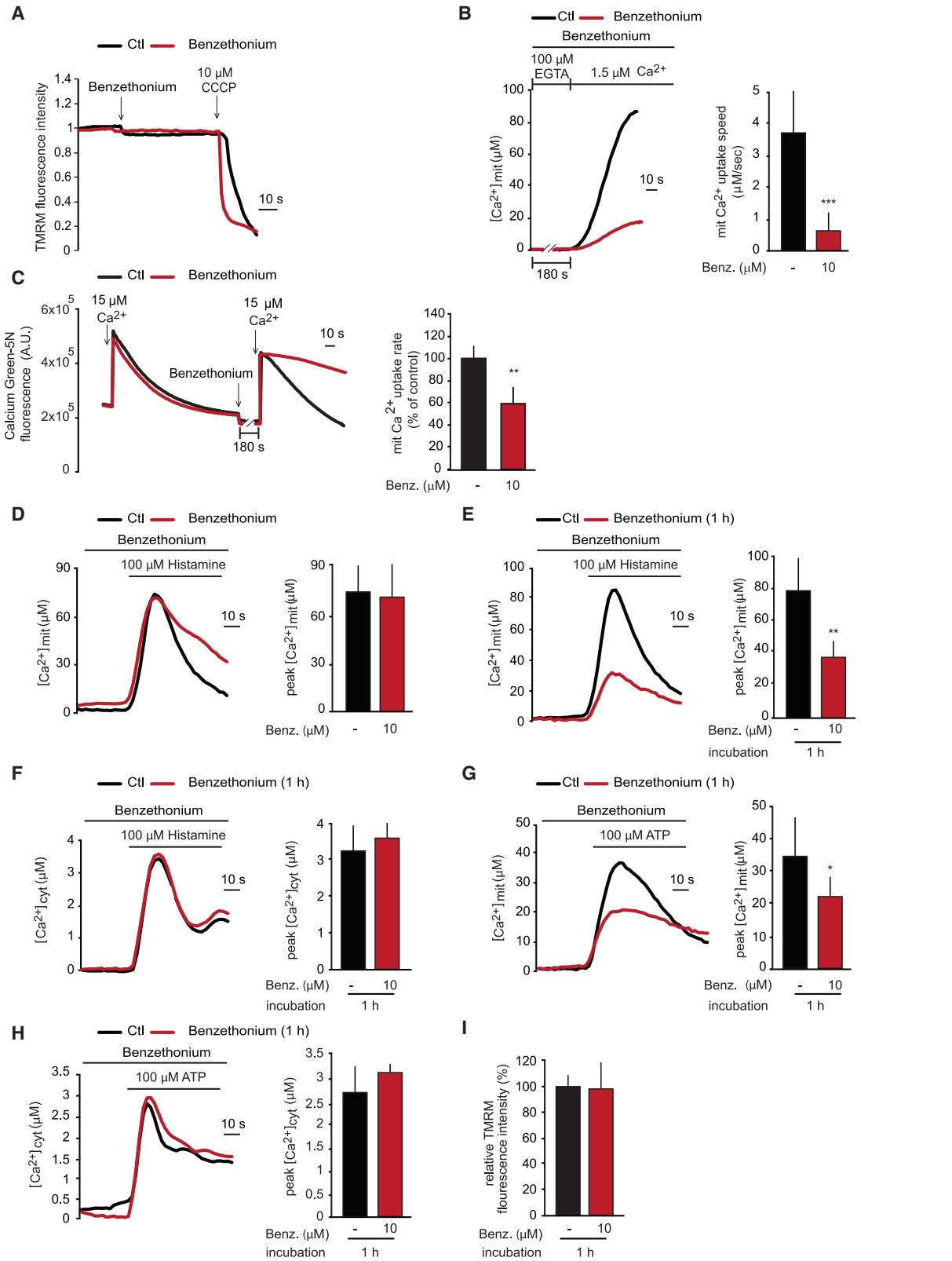

(legend on next page)

21.55 × 10^{-6} M. Benzethonium did not affect cytosolic Ca^{2+} transients (Figure 5F). The effects of benzethonium on mitochondrial Ca^{2+} uptake were independent of the agonist used to trigger IP_3 production, as demonstrated by the fact that ATP stimulation exerted similar effects (Figures 5G and 5H). Importantly, 1-h treatment had no effect on $\Delta\Psi_m$ (Figure 5I).

The data reported in Figures 5D, 5E, and 5G suggest slower mitochondrial Ca^{2+} extrusion in benzethonium-treated cells compared with controls. Thus, we wished to verify whether benzethonium has an inhibitory effect on the mitochondrial Na^{2+}/Ca^{2+} exchanger (NCLX) and whether NCLX activity impinges on drug function. We performed mitochondrial [Ca^{2+}] measurements in the presence of CGP-37157, an inhibitor of NCLX. In intact cells, CGP-37157 increased the mitochondrial [Ca^{2+}] peak upon histamine stimulation, as expected. On the other hand, benzethonium reduced mitochondrial Ca^{2+} accumulation in CGP-37157-treated cells similar to untreated cells, indicating that, independent of NCLX activity, benzethonium prevents mitochondrial Ca^{2+} accumulation (Figure S4A). In line with these data, in permeabilized cells, CGP-37157 increased the speed of mitochondrial Ca^{2+} accumulation but again had no effect on inhibition triggered by benzethonium (Figure S4B). To clarify the effects of benzethonium on NCLX, we added the drug to permeabilized cells in the presence of Ca^{2+} when mitochondrial [Ca^{2+}] had reached the steady state (Figure S4C). CGP-37157 caused a 4-fold increase in mitochondrial [Ca^{2+}] that was reversed suddenly by addition of the MCU inhibitor Ruthenium Red. Moreover, benzethonium caused a 2-fold increase in mitochondrial [Ca^{2+}], indicating that the drug has a dual role, inhibiting the MCU and the NCLX, with an overall effect of reducing mitochondrial Ca^{2+} accumulation upon stimulation.

Benzethonium protects breast cancer cells from apoptotic death and impairs mitochondrial bioenergetics and mitochondrial reactive oxygen species (mROS) production

MCU modulation plays multiple roles in cancer progression. On one hand, mitochondrial Ca^{2+} overload is responsible for apoptotic cell death, and reduced MCU activity has been associated with increased cancer cell survival (Marchi et al., 2013; Hong et al., 2017). On the other hand, MCU activity is required for cancer cell migration, tumor growth, and metastasis formation (Tosatto et al., 2016; Tang et al., 2015; Liu et al., 2020; Zeng et al., 2018; Yu et al., 2017). We demonstrated previously that, in the triple-negative breast cancer cell line MDA-MB-231, MCU silencing decreases colony formation and cell migration with a mechanism that requires mROS and hypoxia-inducible factor 1-alpha (HIF1-α) activity (Tosatto et al., 2016). We thus tested whether benzethonium has similar effects. We measured mitochondrial Ca^{2+} uptake and cytosolic Ca^{2+} transients upon ATP stimulation in drug-treated MDA-MB-231 cells. Compared with vehicle-treated cells, 1 μM benzethonium reduced mitochondrial Ca^{2+} uptake (Figures 6A and 6B) without affecting cytosolic Ca^{2+} transients and $\Delta\Psi_m$ (Figures S5A–S5C). The EC_{50} was 4.53 × 10^{-7} M. In line with the protective role of reduced MCU activity against mitochondrial Ca^{2+} overload (Marchi et al., 2020), benzethonium protected MDA-MB-231 cells from ceramide-induced apoptosis (Figure 6C). We next evaluated the effect of benzethonium on oxidative phosphorylation (OXPHOS) activity and mROS formation. To assess OXPHOS activity, we measured the OCR of MDA-MB-231 cells upon drug treatment. In line with the role of mitochondrial Ca^{2+} uptake in OXPHOS stimulation, 1 μM benzethonium reduced basal, ATP-linked, and maximal respiration (Figure 6D). In addition, in agreement with the reduction in mROS formation upon MCU silencing in MDA-MB-231 cells (Tosatto et al., 2016), 1 μM benzethonium decreased superoxide anion production and mitochondrial H_2O_2 levels (Figure 6E-F). However, the drug had no effect on mitochondrial glutathione disulfide/glutathione (GSSG/GSH), and cytosolic H_2O_2 production was also unaffected (Figures S5D and S5E). Interestingly, 0.5 μM benzethonium, that reduced mitochondrial Ca^{2+} uptake only after 48 h of treatment (Figures 6A and 6B), was inefficient at reducing OCR and mROS formation (Figures 6D–6F), indicating that early inhibition is required.

In line with the effects of MCU silencing or deletion (Tosatto et al., 2016), 1 μM benzethonium reduced MDA-MB-231 colony formation (Figure 7A), cell growth (Figure 7B), and migration (Figure 7C). To verify whether MCU was required, we measured these parameters in *MCU*$^{-/-}$ MDA-MB-231 cells (Tosatto et al.,

Figure 5. Benzethonium is a negative MCU modulator

(A) $\Delta\Psi_m$ measurements in HeLa cells upon treatment with benzethonium or DMSO. Carbonyl cyanide 3-chlorophenylhydrazone (CCCP) was added at the end of the experiment to dissipate $\Delta\Psi_m$.

(B) Mitochondrial Ca^{2+} uptake measurements in permeabilized HeLa cells. Cells were treated with benzethonium or DMSO before (180 s) and during Ca^{2+} perfusion. Left: representative traces. Right: mean $[Ca^{2+}]_{mit}$ speed.

(C) Extramitochondrial Ca^{2+} removal in permeabilized HeLa cells, measured by Calcium Green-5N fluorescence. After addition of a first bolus of $CaCl_2$, benzethonium or DMSO was added. 3 min later, a second bolus of $CaCl_2$ was added. For each sample, the ratio of the two mitochondrial Ca^{2+} uptake rates was calculated. Left: representative traces. Right: percentage of vehicle ratio (control).

(D) Agonist-induced mitochondrial Ca^{2+} uptake in intact HeLa cells. Cells were treated with benzethonium or DMSO before (30 s) and during histamine stimulation. Left: representative traces. Right: mean $[Ca^{2+}]_{mit}$ peaks.

(E) Agonist-induced mitochondrial Ca^{2+} uptake in intact HeLa cells upon benzethonium incubation. Before measurements, cells were treated with benzethonium or DMSO for 1 h. Cells were then kept in benzethonium or DMSO before (30 s) and during histamine stimulation. Left: representative traces. Right: mean $[Ca^{2+}]_{mit}$ peaks.

(F) Agonist-induced cytosolic Ca^{2+} transients in intact HeLa cells upon benzethonium incubation. Before measurements, cells were treated with benzethonium or DMSO for 1 h. Cells were then kept in benzethonium or DMSO before (30 s) and during histamine stimulation. Left: representative traces. Right: mean $[Ca^{2+}]_{cyt}$ peaks.

(G) Agonist-induced mitochondrial Ca^{2+} uptake in intact HeLa cells upon benzethonium incubation. Before measurements, cells were treated with benzethonium or DMSO for 1 h. Cells were then kept in benzethonium or DMSO before (30 s) and during ATP stimulation. Left: representative traces. Right: mean $[Ca^{2+}]_{mit}$ peaks.

(H) Agonist-induced cytosolic Ca^{2+} transients in intact HeLa cells upon benzethonium incubation. Before measurements, cells were treated with benzethonium or DMSO for 1 h. Cells were then kept in benzethonium or DMSO before (30 s) and during ATP stimulation. Left: representative traces. Right: mean $[Ca^{2+}]_{cyt}$ peaks.

(I) $\Delta\Psi_m$ measurements in HeLa cells after 1 h of treatment with benzethonium or DMSO.

Data are presented as mean ± SD. *$p < 0.05$, **$p < 0.01$, ***$p < 0.001$; Student's two-tailed t test except Mann-Whitney rank-sum test for (A), (B), and (H).

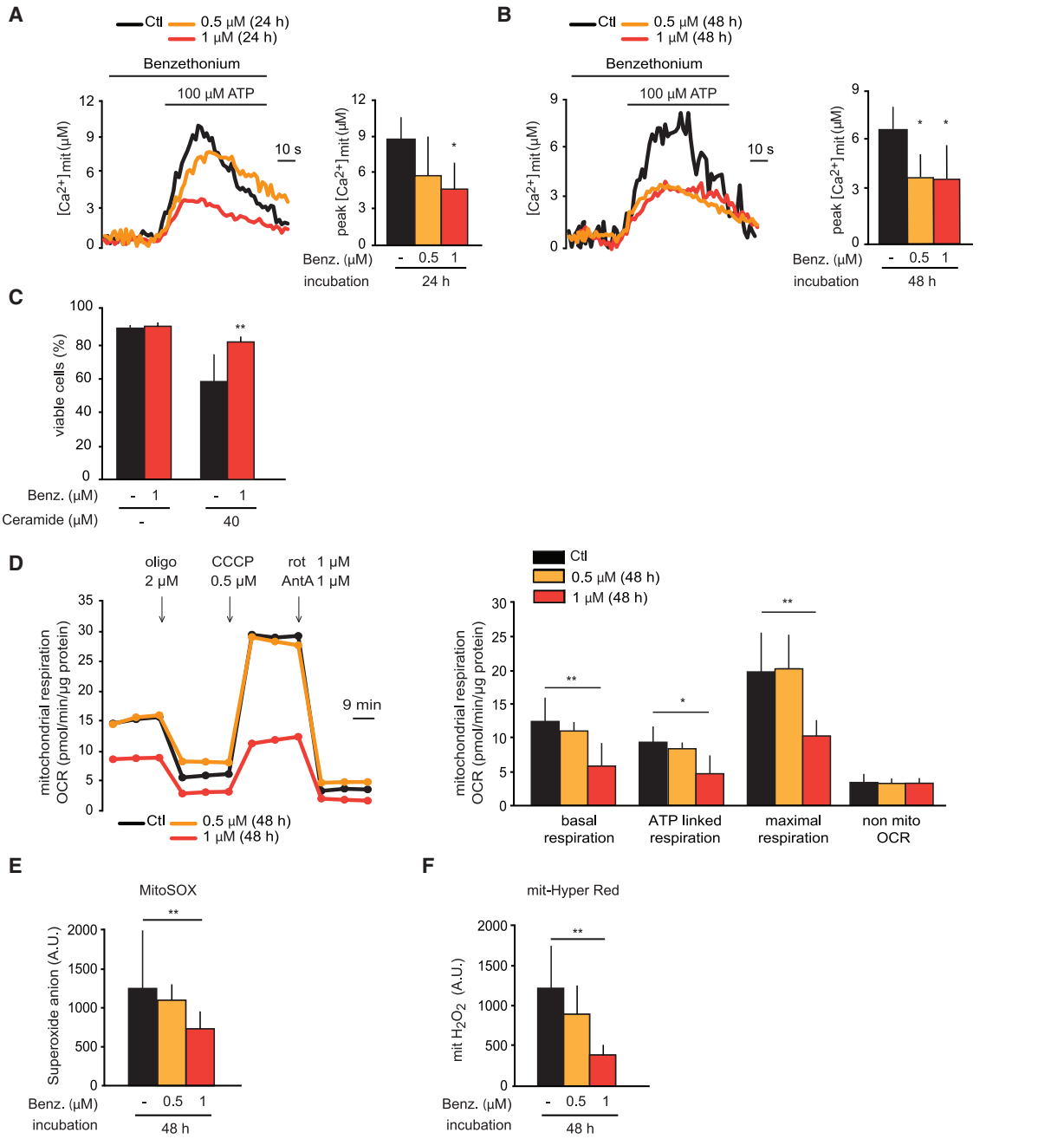

Figure 6. Benzethonium reduces mitochondrial Ca^{2+} uptake, OCR, and mROS production in MDA-MB-231 cells

(A) Agonist-induced mitochondrial Ca^{2+} uptake in MDA-MB-231 cells upon benzethonium treatment. Before measurements, cells were treated with benzethonium or DMSO for 24 h. Cells were then kept in benzethonium or DMSO before (30 s) and during ATP stimulation. Left: representative traces. Right: mean $[Ca^{2+}]_{mit}$ peaks.

(B) Agonist-induced mitochondrial Ca^{2+} uptake in MDA-MB-231 cells upon benzethonium treatment. Before measurements, cells were treated with benzethonium or DMSO for 48 h. Cells were then kept in benzethonium or DMSO before (30 s) and during 100 µM ATP stimulation. Left: representative traces of mitochondrial Ca^{2+} uptake. Right: mean $[Ca^{2+}]_{mit}$ peaks.

(C) Cell viability of benzethonium-treated MDA-MB-231 cells. Cells were treated with benzethonium or DMSO with or without ceramide. 48 h later, viable cells were measured by fluorescence-activated cell sorting (FACS).

(D) OCR measurement in MDA-MB-231 cells upon benzethonium treatment. MDA-MB-231 cells were treated with benzethonium or DMSO, and OCR was measured. To calculate basal and maximal respiration, non-mitochondrial O_2 consumption was subtracted from absolute values. ATP-linked respiration was calculated as the difference between basal and oligomycin-insensitive O_2 consumption. Data are normalized on protein content. Left: representative traces. Right: OCR quantification.

(legend continued on next page)

2016) upon drug treatment. MCU deletion reduced cell growth and migration, as reported previously (Tosatto et al., 2016), and blunted the effects of benzethonium (Figure 7D-E). These results demonstrate that benzethonium inhibits mitochondrial Ca^{2+}-dependent tumor cell growth and migration by negatively modulating the MCU.

DISCUSSION

The MCU is a putative pharmacological target in many pathological conditions, including cardiomyopathies, skeletal muscle diseases, nervous system disorders, hepatopathies, endocrine pancreas deficits, and cancer. Despite the many attempts to develop or identify MCU-targeting lead molecules, clinically approved drugs affecting MCU activity comprise only the antineoplastic drugs mitoxantrone (Arduino et al., 2017) and estrogen receptor modulators (Lobatón et al., 2005). In addition, most MCU-targeting compounds are inhibitors of mitochondrial Ca^{2+} uptake. These molecules are extremely relevant to counteract mitochondrial Ca^{2+} overload, a main trigger of cell death. However, MCU activators may also be relevant in conditions where increased mitochondrial activity is beneficial, including skeletal muscle function, repair of injured plasma membranes, and cell growth. SB202190, specific natural plant flavonoids, and some estrogen receptor modulators are the only known compounds to exert this activity (Montero et al., 2002, 2004; Lobatón et al., 2005). Thus, our purpose was two-fold: we aimed to identify clinically approved MCU-targeting drugs, and we wished to characterize activators and inhibitors of mitochondrial Ca^{2+} uptake.

The high-throughput screening method we applied allowed fast selection of drugs able to specifically modulate mitochondrial Ca^{2+} uptake. However, our screening missed the negative modulation of mitochondrial Ca^{2+} uptake exerted by the MCU inhibitor mitoxantrone (Table S1; Arduino et al., 2017). When tested in the small-scale system, 10 μM mitoxantrone triggered 35% ± 12% reduction in mitochondrial Ca^{2+} uptake and had no effect on cytosolic Ca^{2+} transients, confirming previous data and indicating that mitoxantrone is a false negative hit in our screen.

Furthermore, single-cell $\Delta\Psi_m$ measurements allowed exclusion of false negative modulators. Anti-histamine drugs were excluded directly because they impair not only mitochondrial Ca^{2+} entry but also cytosolic Ca^{2+} transient generation. However, our screening revealed that additional caution must be placed when detecting drugs that interfere with global Ca^{2+} signaling. The case of duloxetine is paradigmatic to illustrate that [Ca^{2+}] measurements, upon stimulation with alternative agonists, are effective to unmask these molecules.

Amorolfine and benzethonium show the main features of MCU-targeting drugs (i.e., modulation of mitochondrial Ca^{2+} uptake in intact and permeabilized cells), without significant effects on cytosolic Ca^{2+} transients and $\Delta\Psi_m$ upon stimulation with different IP_3-generating agonists.

Positive modulation of mitochondrial Ca^{2+} uptake by amorolfine mimics what has been observed previously by genetic manipulation of the MCU in skeletal muscle (Mammucari et al., 2015). Similarly to MCU overexpression, amorolfine has a hypertrophic effect *in vivo*, offering the possibility to use this drug to counteract different conditions characterized by muscle atrophy; e.g., disuse, aging, and neuromuscular disorders. Morphological and molecular analyses of C2C12 myotubes treated with amorolfine indicate that the drug accelerates myotube differentiation, resulting in increased myotube size. The observation that the MCU is required for this effect uncovers an additional role of mitochondrial Ca^{2+} uptake in myotube formation *in vitro*.

It is established that inhibition of mitochondrial Ca^{2+} uptake triggers muscle atrophy. This has been demonstrated in adult skeletal muscle in which the MCU was silenced (Mammucari et al., 2015) or deleted (Gherardi et al., 2019). Similarly, muscle atrophy has been observed in animals in which cytosolic-mitochondria Ca^{2+} coupling was impaired by MICU1 deletion (Debattisti et al., 2019). Finally, treatment with the MICU1-targeting compound MCU-i11 caused a decrease in myotube size (Di Marco et al., 2020). However, MCU silencing per se did not cause C2C12 myotube atrophy, indicating that, in adult muscles, mitochondrial Ca^{2+} decodes multiple signals that are instead dispensable in the cell line. This is most likely the result of the structural and functional properties of the C2C12 cell line compared with animal muscles, including lack of muscle-tendon junctions, innervation and EC coupling, and different mitochondrial positioning.

It is worth noting that functional mitochondrial Ca^{2+} uptake is required not only for maintenance of muscle size and force (Gherardi et al., 2019) but also for plasma membrane integrity, a function that extends beyond muscle cells subjected to damaging lengthening or contraction or affected by dystrophy, and regards additional cell types, including fibroblasts (Horn et al., 2017). In addition, fibrotic stimuli alter channel gating to reduce mitochondrial Ca^{2+} uptake, and MCU deletion impairs fibroblast-to-myofibroblast differentiation, leading to pathological cardiac fibrosis after injury (Lombardi et al., 2019). In this context, amorolfine may be a lead compound to test whether pharmacological treatment with mitochondrial Ca^{2+} uptake-enhancing drugs may be useful in conditions affecting connective tissue, including wound healing and tissue repair.

Our screening revealed benzethonium as a negative modulator of mitochondrial Ca^{2+} accumulation. However, the low cell permeability of benzethonium must be considered. For example, in I/R injury of the heart, mitochondrial Ca^{2+} entry and increased reactive oxygen species (ROS) formation result

(E) Mitochondrial superoxide anion in MDA-MB-231 cells upon benzethonium treatment. MDA-MB-231 cells were treated with benzethonium or DMSO before (48 h) and during measurements. The day of the experiment, cells were loaded with MitoSOX, and superoxide anion levels were measured. Results are expressed as MitoSOX fluorescence.

(F) Mitochondrial H_2O_2 in MDA-MB-231 cells upon benzethonium treatment. MDA-MB-231 cells were transfected with plasmids encoding mitHyper Red and treated with benzethonium or DMSO. 48 h later, mitochondrial H_2O_2 was measured. Results are expressed as mitHyper Red fluorescence.

Data are presented as mean – SD. *$p < 0.05$, **$p < 0.01$; one-way ANOVA except two-way ANOVA for (C).

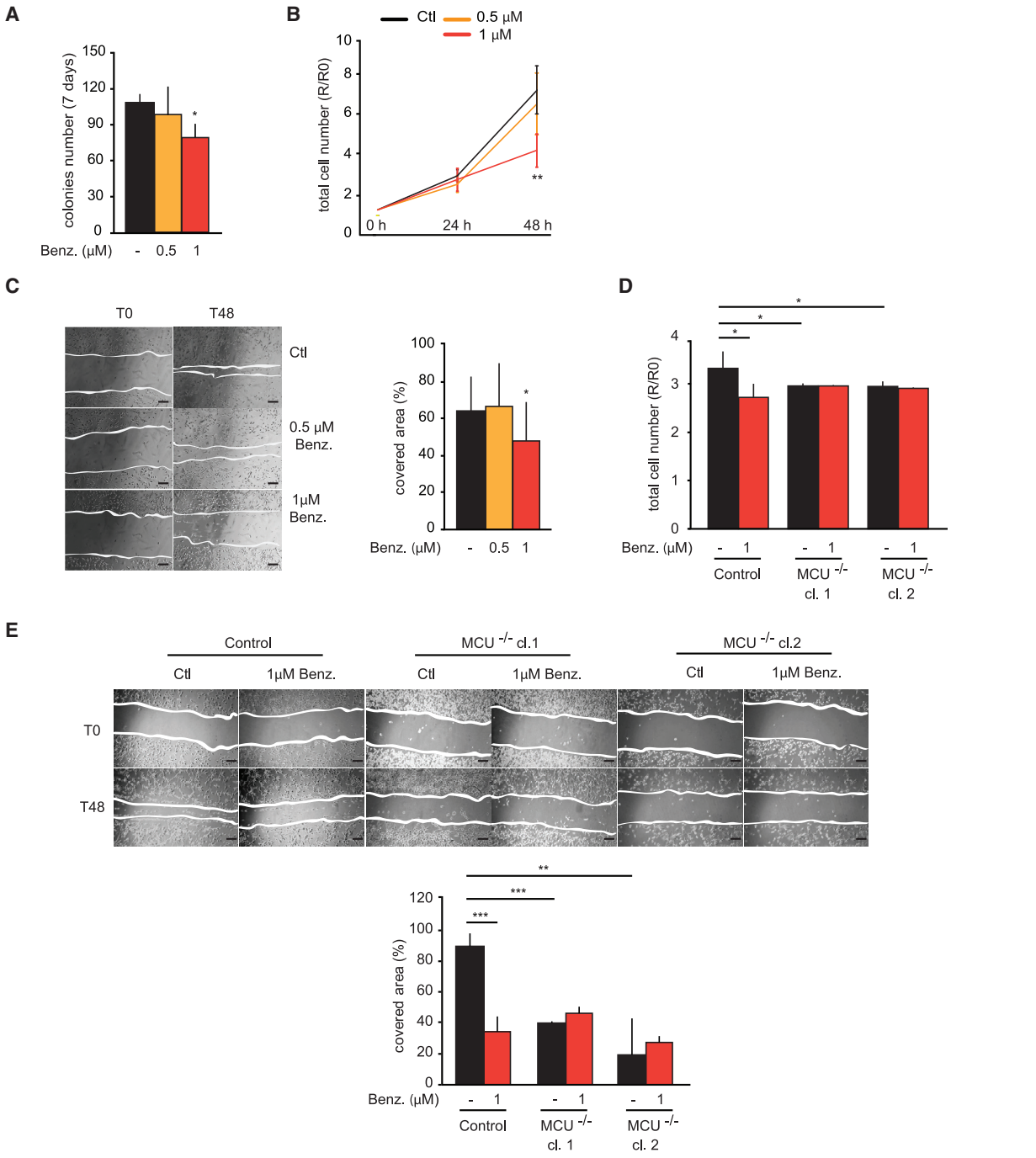

Figure 7. Benzethonium inhibits breast cancer cell growth and migration by negatively modulating MCU activity

(A) MDA-MB-231 clonogenic potential upon benzethonium treatment. 10^3 cells/well were seeded in a 6-well plate. 24 h later, cells were incubated with benzethonium or DMSO. 7 days later, colonies containing ≥ 30 cells were counted.

(B) MDA-MB-231 cell proliferation upon benzethonium treatment. Cells were treated with benzethonium or DMSO. Cells were counted every 24 h. Results are expressed as the ratio R/R0, where R is the number of cells at time (T), and R0 is the number of cells at time 0.

(C) MDA-MB-231 cell migration upon benzethonium treatment. When cells plated in a monolayer reached 90% confluency, they were treated with benzethonium or DMSO, and a linear scratch was made (T0 time point). 24 h later, benzethonium-containing medium was replaced. 48 h after scratching (T48), the area covered by cells was measured and expressed as percentage relative to T0. Left: representative images. Right: quantification. Scale bar, 100 μm.

(D) Cell proliferation upon benzethonium treatment. Cells were treated with benzethonium or DMSO and counted 48 h later. Results are expressed as the ratio R/R0, where R is the number of cells at T48, and R0 is the number of cells at T0.

(legend continued on next page)

in the opening of the mitochondrial permeability transition pore (mPTP) compromising cell survival (Andreadou et al., 2020). Accordingly, conditional cardiac-specific MCU deletion had a beneficial effect on I/R injury (Kwong et al., 2015; Luongo et al., 2015). However, physiological ROS levels underlie protective ischemic pre-conditioning (Andreadou et al., 2020). Thus, for use of pharmacological agents impinging on mitochondrial Ca^{2+} uptake and mROS production, timely and fine-tuned modulation of these critical checkpoints must be achieved.

A second issue was the inhibitory effect of benzethonium on the NCLX. Nonetheless, differently from CGP-37157, benzethonium only modestly inhibited Ca^{2+} extrusion, indicating that inhibition of the MCU prevailed.

We analyzed the effects of benzethonium in cancer cell growth and migration, properties known to be controlled by the MCU (Tosatto et al., 2016; Tang et al., 2015; Liu et al., 2020; Zeng et al., 2018; Yu et al., 2017; Ren et al., 2017). Negative modulation of mitochondrial Ca^{2+} uptake by benzethonium mimicked what has been observed previously by genetic manipulation of the MCU (Tosatto et al., 2016), and the MCU was required for drug effects.

Mitochondrial Ca^{2+} uptake plays a dual role in cancer progression. On one hand, mitochondrial Ca^{2+} homeostasis is required for cell growth and tumor progression, as mentioned above. On the other hand, mitochondrial Ca^{2+} overload is a trigger of apoptotic cell death (Marchi et al., 2019). Accordingly, microRNA targeting of mitochondrial Ca^{2+} signaling favors survival of colon cancer cells (Marchi et al., 2013). However, benzethonium has been suggested as an anti-cancer drug because of its ability to induce apoptosis in different cancer cell lines, although at concentrations higher than the one used in our study (Huang et al., 2019; Yip et al., 2006). In addition, Yip et al. (2006) reported an effect of benzethonium on cytosolic Ca^{2+} and on $\Delta\Psi_m$. Thus, whether benzethonium is an inhibitor or a trigger of apoptotic cell death in the MDA-MB-231 cell line was an open question. Our data excluded induction of apoptosis as a trigger of impaired cell growth and migration. Rather, in accordance with the pro-apoptotic function of excessive mitochondrial Ca^{2+} entry, benzethonium protected cells from ceramide-induced death. We also did not observe any effect on the overall cytosolic Ca^{2+} or on $\Delta\Psi_m$. This apparent discrepancy is explained by the use of different drug concentrations. Similarly to previous reports (Huang et al., 2019; Yip et al., 2006), we indeed observed that 10 μM benzethonium triggers MDA-MB-231 cell death (data not shown). Finally, benzethonium and other quaternary ammonium compounds inhibit complex I-driven ATP synthesis *in vitro* when cybrid cells containing a Leber hereditary optic neuropathy (LHON) mutation were incubated with 10 μM of the drug for 22 h (Datta et al., 2017). However, as reported in Table S1, the effects on mitochondrial Ca^{2+} uptake are not shared with other quaternary ammonium compounds, including benzalkonium. In addition, the functional effects of benzethonium are already observed at 1 μM, a concentration an order of magnitude lower than what is required to observe the effects on complex I-driven ATP production. Thus, although benzethonium could have multiple mechanisms in different cell lines and at different concentrations, our data support the specific role of mitochondrial Ca^{2+} uptake inhibition in triple-negative breast cancer.

In conclusion, amorolfine and benzethonium are lead drugs for pharmacological modulation of mitochondrial Ca^{2+} uptake in pathophysiological settings in which genetic manipulation of the MCU is challenging.

STAR★METHODS

Detailed methods are provided in the online version of this paper and include the following:

- KEY RESOURCES TABLE
- RESOURCE AVAILABILITY
  - Lead contact
  - Materials availability
  - Data and code availability
- EXPERIMENTAL MODEL AND SUBJECT DETAILS
  - Mice
  - Cell lines
  - Primary cell cultures
- METHOD DETAILS
  - Plasmids and *in vitro* transfection
  - Construction of adenoviral vectors for 4mtGCamp6f probe
  - C2C12 Adenoviral infection
  - *In vivo* DNA transfection of mouse skeletal muscles and myofiber isolation
  - Drugs
  - High-throughput Ca^{2+} measurements and data analysis
  - Small-scale Ca^{2+} measurements
  - Mitochondrial Ca^{2+} uptake measurements in permeabilized HeLa cells by Calcium Green-5N fluorescence
  - EC_{50} calculation
  - Oxygen consumption rate (OCR) measurements
  - ROS production measurement
  - Mitochondrial membrane potential ($\Delta\Psi_m$) measurements
  - C2C12 morphological analysis
  - Myofiber size analysis
  - Cell viability assays
  - Cell proliferation assay
  - Clonogenic assay
  - Migration assay
  - RNA extraction, reverse transcription, and quantitative real time PCR
  - Western blotting and antibodies
- QUANTIFICATION AND STATISTICAL ANALYSIS

(E) Cell migration upon benzethonium treatment. When cells plated in a monolayer reached 90% confluence, they were treated with benzethonium or DMSO, and a linear scratch was made (T0). 24 h later, benzethonium-containing medium was replaced. 48 h after scratching (T48), the area covered by cells was measured and expressed as percentage relative to T0. Left: representative images. Right: quantification. Scale bar, 100 μm.
Data are presented as mean ± SD. *p < 0.05, **p < 0.01, ***p < 0.001; two-way ANOVA except one-way ANOVA for (A) and (C).

SUPPLEMENTAL INFORMATION

Supplemental information can be found online at https://doi.org/10.1016/j.celrep.2021.109275.

ACKNOWLEDGMENTS

The project was supported by funding from the French Muscular Dystrophy Association (22493 to C.M.), the Italian Association for Cancer Research (AIRC 22759 to R.R.), the Italian Telethon Association (GGP16029 to R.R.), the Italian Ministry of Health (RF-2016-02363566 to R.R.), the Cariparo Foundation (to R.R.), and the UK Medical Research Council (MC_U12266B to J.K.V. and R.K.). The authors are grateful to Diego De Stefani for insightful discussions.

AUTHOR CONTRIBUTIONS

A.D.M. performed most of the experiments. A.T. performed high-throughput screening. J.M.H., J.K.V., and R.K. analyzed the screening. D.V.R. produced Ad-4mtGCaMP6f. G.S. supervised the screening analysis. G.C., R.R., G.S., and C.M. conceived the research. C.M. directed the project. A.D.M., G.S., and C.M. wrote the paper.

DECLARATION OF INTERESTS

The authors declare no competing interests.

Received: October 14, 2020
Revised: May 10, 2021
Accepted: May 28, 2021
Published: June 22, 2021

REFERENCES

Andreadou, I., Schulz, R., Papapetropoulos, A., Turan, B., Ytrehus, K., Ferdinandy, P., Daiber, A., and Di Lisa, F. (2020). The role of mitochondrial reactive oxygen species, NO and H_2 S in ischaemia/reperfusion injury and cardioprotection. J. Cell. Mol. Med. *24*, 6510–6522.

Arduino, D.M., Wettmarshausen, J., Vais, H., Navas-Navarro, P., Cheng, Y., Leimpek, A., Ma, Z., Delrio-Lorenzo, A., Giordano, A., Garcia-Perez, C., et al. (2017). Systematic Identification of MCU Modulators by Orthogonal Interspecies Chemical Screening. Mol. Cell *67*, 711–723.e7.

Baughman, J.M., Perocchi, F., Girgis, H.S., Plovanich, M., Belcher-Timme, C.A., Sancak, Y., Bao, X.R., Strittmatter, L., Goldberger, O., Bogorad, R.L., et al. (2011). Integrative genomics identifies MCU as an essential component of the mitochondrial calcium uniporter. Nature *476*, 341–345.

Brini, M., Marsault, R., Bastianutto, C., Alvarez, J., Pozzan, T., and Rizzuto, R. (1995). Transfected aequorin in the measurement of cytosolic Ca2+ concentration ([Ca2+]c). A critical evaluation. J. Biol. Chem. *270*, 9896–9903.

Csordás, G., Golenár, T., Seifert, E.L., Kamer, K.J., Sancak, Y., Perocchi, F., Moffat, C., Weaver, D., Perez, S.F., Bogorad, R., et al. (2013). MICU1 controls both the threshold and cooperative activation of the mitochondrial Ca^{2+} uniporter. Cell Metab. *17*, 976–987.

Datta, S., He, G., Tomilov, A., Sahdeo, S., Denison, M.S., and Cortopassi, G. (2017). In vitro evaluation of mitochondrial function and estrogen signaling in cell lines exposed to the antiseptic cetylpyridinium chloride. Environ. Health Perspect. *125*, 087015.

De Stefani, D., Raffaello, A., Teardo, E., Szabò, I., and Rizzuto, R. (2011). A forty-kilodalton protein of the inner membrane is the mitochondrial calcium uniporter. Nature *476*, 336–340.

Debattisti, V., Horn, A., Singh, R., Seifert, E.L., Hogarth, M.W., Mazala, D.A., Huang, K.T., Horvath, R., Jaiswal, J.K., and Hajnóczky, G. (2019). Dysregulation of Mitochondrial Ca^{2+} Uptake and Sarcolemma Repair Underlie Muscle Weakness and Wasting in Patients and Mice Lacking MICU1. Cell Rep. *29*, 1274–1286.e6.

Di Marco, G., Vallese, F., Jourde, B., Bergsdorf, C., Sturlese, M., De Mario, A., Techer-Etienne, V., Haasen, D., Oberhauser, B., Schleeger, S., et al. (2020). A High-Throughput Screening Identifies MICU1 Targeting Compounds. Cell Rep. *30*, 2321–2331.e6.

Emerson, J., Clarke, M.J., Ying, W.L., and Sanadi, D.R. (1993). The Component of "Ruthenium Red" Responsible for Inhibition of Mitochondrial Calcium Ion Transport. Spectra, Electrochemistry, and Aquation Kinetics. Crystal Structure of μ-O-[(HCO2)(NH3)4Ru]2Cl3. J. Am. Chem. Soc. *115*, 11799–11805.

Ermakova, Y.G., Bilan, D.S., Matlashov, M.E., Mishina, N.M., Markvicheva, K.N., Subach, O.M., Subach, F.V., Bogeski, I., Hoth, M., Enikolopov, G., and Belousov, V.V. (2014). Red fluorescent genetically encoded indicator for intracellular hydrogen peroxide. Nat. Commun. *5*, 5222.

Feno, S., Di Marco, G., De Mario, A., Monticelli, H., and Reane, D.V. (2019). High-Throughput Screening Using Photoluminescence Probe to Measure Intracellular Calcium Levels. Methods Mol. Biol. *1925*, 1–14.

Gherardi, G., Nogara, L., Ciciliot, S., Fadini, G.P., Blaauw, B., Braghetta, P., Bonaldo, P., De Stefani, D., Rizzuto, R., and Mammucari, C. (2019). Loss of mitochondrial calcium uniporter rewires skeletal muscle metabolism and substrate preference. Cell Death Differ. *26*, 362–381.

Gutscher, M., Pauleau, A.L., Marty, L., Brach, T., Wabnitz, G.H., Samstag, Y., Meyer, A.J., and Dick, T.P. (2008). Real-time imaging of the intracellular glutathione redox potential. Nat. Methods *5*, 553–559.

Hong, Z., Chen, K.H., DasGupta, A., Potus, F., Dunham-Snary, K., Bonnet, S., Tian, L., Fu, J., Breuils-Bonnet, S., Provencher, S., et al. (2017). MicroRNA-138 and MicroRNA-25 down-regulate mitochondrial calcium uniporter, causing the pulmonary arterial hypertension cancer phenotype. Am. J. Respir. Crit. Care Med. *195*, 515–529.

Horn, A., Van der Meulen, J.H., Defour, A., Hogarth, M., Sreetama, S.C., Reed, A., Scheffer, L., Chandel, N.S., and Jaiswal, J.K. (2017). Mitochondrial redox signaling enables repair of injured skeletal muscle cells. Sci. Signal. *10*, 139–148.

Huang, X.H., Wang, Y., Hong, P., Yang, J., Zheng, C.C., Yin, X.F., Song, W.B., Xu, W.W., Li, B., and He, Q.Y. (2019). Benzethonium chloride suppresses lung cancer tumorigenesis through inducing p38-mediated cyclin D1 degradation. Am. J. Cancer Res. *9*, 2397–2412.

Kon, N., Murakoshi, M., Isobe, A., Kagechika, K., Miyoshi, N., and Nagayama, T. (2017). DS16570511 is a small-molecule inhibitor of the mitochondrial calcium uniporter. Cell Death Discov. *3*, 17045.

Kwong, J.Q., Lu, X., Correll, R.N., Schwanekamp, J.A., Vagnozzi, R.J., Sargent, M.A., York, A.J., Zhang, J., Bers, D.M., and Molkentin, J.D. (2015). The Mitochondrial Calcium Uniporter Selectively Matches Metabolic Output to Acute Contractile Stress in the Heart. Cell Rep. *12*, 15–22.

Lewis-Smith, D., Kamer, K.J., Griffin, H., Childs, A.M., Pysden, K., Titov, D., Duff, J., Pyle, A., Taylor, R.W., Yu-Wai-Man, P., et al. (2016). Homozygous deletion in MICU1 presenting with fatigue and lethargy in childhood. Neurol. Genet. *2*, e59.

Liu, Y., Jin, M., Wang, Y., Zhu, J., Tan, R., Zhao, J., Ji, X., Jin, C., Jia, Y., Ren, T., and Xing, J. (2020). MCU-induced mitochondrial calcium uptake promotes mitochondrial biogenesis and colorectal cancer growth. Signal Transduct. Target. Ther. *5*, 59.

Lobatón, C.D., Vay, L., Hernández-Sanmiguel, E., Santodomingo, J., Moreno, A., Montero, M., and Alvarez, J. (2005). Modulation of mitochondrial Ca(2+) uptake by estrogen receptor agonists and antagonists. Br. J. Pharmacol. *145*, 862–871.

Logan, C.V., Szabadkai, G., Sharpe, J.A., Parry, D.A., Torelli, S., Childs, A.-M.M., Kriek, M., Phadke, R., Johnson, C.A., Roberts, N.Y., et al.; UK10K Consortium (2014). Loss-of-function mutations in MICU1 cause a brain and muscle disorder linked to primary alterations in mitochondrial calcium signaling. Nat. Genet. *46*, 188–193.

Lombardi, A.A., Gibb, A.A., Arif, E., Kolmetzky, D.W., Tomar, D., Luongo, T.S., Jadiya, P., Murray, E.K., Lorkiewicz, P.K., Hajnóczky, G., et al. (2019).

Mitochondrial calcium exchange links metabolism with the epigenome to control cellular differentiation. Nat. Commun. *10*, 4509.

Luongo, T.S., Lambert, J.P., Yuan, A., Zhang, X., Gross, P., Song, J., Shanmughapriya, S., Gao, E., Jain, M., Houser, S.R., et al. (2015). The Mitochondrial Calcium Uniporter Matches Energetic Supply with Cardiac Workload during Stress and Modulates Permeability Transition. Cell Rep. *12*, 23–34.

Mallilankaraman, K., Doonan, P., Cárdenas, C., Chandramoorthy, H.C., Müller, M., Miller, R., Hoffman, N.E., Gandhirajan, R.K., Molgó, J., Birnbaum, M.J., et al. (2012). MICU1 is an essential gatekeeper for MCU-mediated mitochondrial Ca(2+) uptake that regulates cell survival. Cell *151*, 630–644.

Mammucari, C., Gherardi, G., Zamparo, I., Raffaello, A., Boncompagni, S., Chemello, F., Cagnin, S., Braga, A., Zanin, S., Pallafacchina, G., et al. (2015). The mitochondrial calcium uniporter controls skeletal muscle trophism in vivo. Cell Rep. *10*, 1269–1279.

Marchi, S., Lupini, L., Patergnani, S., Rimessi, A., Missiroli, S., Bonora, M., Bononi, A., Corrà, F., Giorgi, C., De Marchi, E., et al. (2013). Downregulation of the mitochondrial calcium uniporter by cancer-related miR-25. Curr. Biol. *23*, 58–63.

Marchi, S., Vitto, V.A.M., Danese, A., Wieckowski, M.R., Giorgi, C., and Pinton, P. (2019). Mitochondrial calcium uniporter complex modulation in cancerogenesis. Cell Cycle *18*, 1068–1083.

Marchi, S., Giorgi, C., Galluzzi, L., and Pinton, P. (2020). Ca^{2+} Fluxes and Cancer. Mol. Cell *78*, 1055–1069.

Matlib, M.A., Zhou, Z., Knight, S., Ahmed, S., Choi, K.M., Krause-Bauer, J., Phillips, R., Altschuld, R., Katsube, Y., Sperelakis, N., and Bers, D.M. (1998). Oxygen-bridged dinuclear ruthenium amine complex specifically inhibits Ca2+ uptake into mitochondria in vitro and in situ in single cardiac myocytes. J. Biol. Chem. *273*, 10223–10231.

Montero, M., Lobaton, C.D., Moreno, A., and Alvarez, J. (2002). A novel regulatory mechanism of the mitochondrial Ca2+ uniporter revealed by the p38 mitogen-activated protein kinase inhibitor SB202190. FASEB J. *16*, 1955–1957.

Montero, M., Lobatón, C.D., Hernández-Sanmiguel, E., Santodomingo, J., Vay, L., Moreno, A., and Alvarez, J. (2004). Direct activation of the mitochondrial calcium uniporter by natural plant flavonoids. Biochem. J. *384*, 19–24.

Musa, S., Eyaid, W., Kamer, K., Ali, R., Al-Mureikhi, M., Shahbeck, N., Al Mesaifri, F., Makhseed, N., Mohamed, Z., AlShehhi, W.A., et al. (2018). A Middle Eastern Founder Mutation Expands the Genotypic and Phenotypic Spectrum of Mitochondrial MICU1 Deficiency: A Report of 13 Patients. JIMD reports *43*, 79–83.

Patron, M., Checchetto, V., Raffaello, A., Teardo, E., Vecellio Reane, D., Mantoan, M., Granatiero, V., Szabò, I., De Stefani, D., and Rizzuto, R. (2014). MICU1 and MICU2 finely tune the mitochondrial Ca2+ uniporter by exerting opposite effects on MCU activity. Mol. Cell *53*, 726–737.

Ren, T., Zhang, H., Wang, J., Zhu, J., Jin, M., Wu, Y., Guo, X., Ji, L., Huang, Q., Zhang, H., et al. (2017). MCU-dependent mitochondrial Ca^{2+} inhibits NAD^{+}/SIRT3/SOD2 pathway to promote ROS production and metastasis of HCC cells. Oncogene *36*, 5897–5909.

Rizzuto, R., Simpson, A.W.M., Brini, M., and Pozzan, T. (1992). Rapid changes of mitochondrial Ca2+ revealed by specifically targeted recombinant aequorin. Nature *358*, 325–327.

Rizzuto, R., De Stefani, D., Raffaello, A., and Mammucari, C. (2012). Mitochondria as sensors and regulators of calcium signalling. Nat. Rev. Mol. Cell Biol. *13*, 566–578.

Santo-Domingo, J., Vay, L., Hernández-Sanmiguel, E., Lobatón, C.D., Moreno, A., Montero, M., and Alvarez, J. (2007). The plasma membrane Na+/Ca2+ exchange inhibitor KB-R7943 is also a potent inhibitor of the mitochondrial Ca2+ uniporter. Br. J. Pharmacol. *151*, 647–654.

Schindelin, J., Arganda-Carreras, I., Frise, E., Kaynig, V., Longair, M., Pietzsch, T., Preibisch, S., Rueden, C., Saalfeld, S., Schmid, B., et al. (2012). Fiji: an open-source platform for biological-image analysis. Nat. Methods *9*, 676–682.

Tang, S., Wang, X., Shen, Q., Yang, X., Yu, C., Cai, C., Cai, G., Meng, X., and Zou, F. (2015). Mitochondrial Ca^{2+} uniporter is critical for store-operated Ca^{2+} entry-dependent breast cancer cell migration. Biochem. Biophys. Res. Commun. *458*, 186–193.

Tosatto, A., Sommaggio, R., Kummerow, C., Bentham, R.B., Blacker, T.S., Berecz, T., Duchen, M.R., Rosato, A., Bogeski, I., Szabadkai, G., et al. (2016). The mitochondrial calcium uniporter regulates breast cancer progression via HIF-1α. EMBO Mol. Med. *8*, 569–585.

Tosatto, A., Rizzuto, R., and Mammucari, C. (2017). Ca^{2+} Measurements in Mammalian Cells with Aequorin-based Probes. Bio Protoc. *7*, e2155.

Woods, J.J., Nemani, N., Shanmughapriya, S., Kumar, A., Zhang, M., Nathan, S.R., Thomas, M., Carvalho, E., Ramachandran, K., Srikantan, S., et al. (2019). A Selective and Cell-Permeable Mitochondrial Calcium Uniporter (MCU) Inhibitor Preserves Mitochondrial Bioenergetics after Hypoxia/Reoxygenation Injury. ACS Cent. Sci. *5*, 153–166.

Ying, W.L., Emerson, J., Clarke, M.J., and Sanadi, D.R. (1991). Inhibition of mitochondrial calcium ion transport by an oxo-bridged dinuclear ruthenium ammine complex. Biochemistry *30*, 4949–4952.

Yip, K.W., Mao, X., Au, P.Y.B., Hedley, D.W., Chow, S., Dalili, S., Mocanu, J.D., Bastianutto, C., Schimmer, A., and Liu, F.F. (2006). Benzethonium chloride: a novel anticancer agent identified by using a cell-based small-molecule screen. Clin. Cancer Res. *12*, 5557–5569.

Yu, C., Wang, Y., Peng, J., Shen, Q., Chen, M., Tang, W., Li, X., Cai, C., Wang, B., Cai, S., et al. (2017). Mitochondrial calcium uniporter as a target of microRNA-340 and promoter of metastasis via enhancing the Warburg effect. Oncotarget *8*, 83831–83844.

Zeng, F., Chen, X., Cui, W., Wen, W., Lu, F., Sun, X., Ma, D., Yuan, Y., Li, Z., Hou, N., et al. (2018). RIPK1 binds MCU to mediate induction of mitochondrial Ca2+ uptake and promotes colorectal oncogenesis. Cancer Res. *78*, 2876–2885.

STAR★METHODS

KEY RESOURCES TABLE

REAGENT or RESOURCE	SOURCE	IDENTIFIER
Antibodies		
anti-MCU	Sigma	Cat# HPA016480; RRID:AB_2071893
anti-actin	Santa Cruz Biotechnology	Cat# SC56459; RRID AB_830981
Horseradish peroxidase-conjugated anti-rabbit-IgG	Santa Cruz Biotechnology	Cat# SC2004; RRID AB_631746
Horseradish peroxidase-conjugated anti-mouse-IgG	Santa Cruz Biotechnology	Cat# SC2005; RRID AB_631736
ani-Laminin	Sigma-Aldrich	Cat# L9393; RRID AB_477163
Alexa Fluor 488-conjugated secondary antibody	Thermo Fisher Scientific	Cat# A21206; RRID AB_2535792
Bacterial and virus strains		
Adenovirus mCherry-U6-scramble-shRNA	Vector Biolabs	Cat# 1781
Adenovirus mCherry-U6-m-MCU-shRNA	Vector Biolabs	Cat# 254662
Adenovirus 4mtGCaMP6f	This manuscript	N/A
Chemicals, peptides, and recombinant proteins		
Caffeine	Sigma Aldrich	CAT# 58082
Histamine dihydrochloride	Sigma Aldrich	CAT# H7250
ATP	Sigma Aldrich	CAT# 34369-07-8
Digitonin	Sigma Aldrich	CAT# 11024-24-1
Charbachol	Sigma Aldrich	CAT# Y0000113
TMRM	Thermo Fisher Scientific	CAT# T668
Coelenterazine H	Regis Technology	CAT# 50909-86-9
Amorolfine hydrochloride	Sigma Aldrich	CAT# Y0001795
Benzethonium chloride	Sigma Aldrich	CAT# B8879
Duloxetine hydrochloride	Sigma Aldrich	CAT# PHR1865
Pharmakon-1600 collection	Microsource Discovery System Inc.	N/A
Hyaluronidase from bovine testis	Sigma Aldrich	CAT# H4272
Dimethyl sulfoxide	Sigma Aldrich	CAT# D2438
4-Methyl-*N*-(phenylmethyl)benzenesulfonamide	Tocris	CAT# 1870
FURA-2 AM	Thermo Fisher Scientific	CAT# F1221
Carbonyl cyanide 3-chlorophenylhydrazone	Sigma Aldrich	CAT# C2759
MitoSOX	Thermo Fisher Scientific	CAT# M36008
CellTiter 96 Aqueous One Solution Cell Proliferation Assay (MTS)	Promega	CAT# G3582
eBioscience Annexin V Apoptosis Detection Kit FITC	Invitrogen	CAT# 88-8005-72
Oligomycin	Sigma Aldrich	CAT# 75351
Antimycin A	Sigma Aldrich	CAT# A8674
Rotenone	Sigma Aldrich	CAT# R8875
Hydrogen peroxide	Sigma Aldrich	CAT# 386790-M
Calcium Green-5N	Invitrogen	CAT# C3737
CGP-37157	Sigma Aldrich	CAT# C8874
Experimental models: cell lines		
HeLa	ATCC	Cat# CCL-2, RRID:CVCL_0030

(*Continued on next page*)

Continued

REAGENT or RESOURCE	SOURCE	IDENTIFIER
MDA-MB-231	NCI-DTP	Cat# MDA-MB-231, RRID:CVCL_0062
C2C12	ATCC	Cat# CRL-1772
$MCU^{-/-}$ MDA-MB-231 clones	available upon request	Tosatto et al., 2016
Experimental models: organisms/strains		
CD-1 IGS mouse	Charles River Laboratories	Cat# Crl:CD1(ICR)
Oligonucleotides		
Primer Myf5 forward: 5′-GAGCTGC TGAGGGAACAGGTGGAGA-3′	Integrated DNA Technologies	N/A
Primer Myf5 reverse: 5′-GTTCTTTCG GGACCAGACAGGGCTG-3′	Integrated DNA Technologies	N/A
Primer GAPDH forward: 5′-CACC ATCTTCCAGGAGCGAG-3′	Integrated DNA Technologies	N/A
Primer GAPDH reverse: 5′-CCTTCT CCATGGTGGTGAAGAC-3′	Integrated DNA Technologies	N/A
Primer MyoD forward: 5′-CTCT GATGGCATGATGGAT-3′	Integrated DNA Technologies	N/A
Primer MyoD reverse: 5′-GTGG AGATGCGCTCCACTAT-3′	Integrated DNA Technologies	N/A
Recombinant DNA		
pcDNA3.1-4mtGCaMP6f	Mammucari Lab; Tosatto et al., 2016	N/A
mitAEQ-mut	Rizzuto et al., 1992	N/A
cytAEQ	Brini et al., 1995	N/A
mit-HyperRed	Ermakova et al., 2014	N/A
HyperRed	Ermakova et al., 2014	Addgene Cat# 48249
pLPCXmitGrx1-roGFP2	Gutscher et al., 2008	Addgene Cat# 64977
Software and algorithms		
cellHTS2 R	Bioconductor	10.18129/B9.bioc.cellHTS2
FACS Canto II	BD Bioscience	https://www.bdbiosciences.com/en-us/instruments/research-instruments/research-software/flow-cytometry-acquisition/facsdiva-software
TScratch	CSElab	https://www.cse-lab.ethz.ch/software/
Sigma Plot 12.0	N/A	https://systatsoftware.com/products/sigmaplot/sigmaplot-statistical-analysis/
Fiji	ImageJ	Schindelin et al., 2012; https://imagej.nih.gov/ij/
GraphPad Prism8	Graph Pad	https://www.graphpad.com/scientific-software/prism/

RESOURCE AVAILABILITY

Lead contact

Further information and requests for resources and reagents should be directed to and will be fulfilled by the lead contact, Cristina Mammucari (cristina.mammucari@unipd.it).

Materials availability

All unique/stable reagents generated in this study are available from the lead contact without restriction.

Data and code availability

This study did not generate any unique datasets or code.

EXPERIMENTAL MODEL AND SUBJECT DETAILS

Mice

All animal experiments were approved by the internal Animal Welfare Body and the Italian Ministry of Health and performed in accordance with the Italian law D. L.vo n_26/2014. Adult 2-4 month old CD1 male mice (Charles River) were housed in conventional cages regularly supplied with environmental enrichment, water bottles and *ad libitum* food. Daily oversight and care was provided by specialized veterinarians, trained technicians and animal husbandry staff.

Cell lines

HeLa and C2C12 cells were cultured in Dulbecco's modified Eagle's medium (DMEM) (Life Technologies). MDA-MB-231 cells and MCU$^{-/-}$ MDA-MB-231 clones (Tosatto et al., 2016) were cultured in DMEM-F12 (Life Technologies). All media were supplemented with 10% FBS, 100 U/mL penicillin and 100 mg/mL streptomycin. Cells were maintained at 37°C and 5% CO_2 incubator. To induce C2C12 myotube formation, growth medium was replaced with 2% horse serum (HS)-containing medium.

Primary cell cultures

Adult male CD1 mouse myofibers were cultured in DMEM with HEPES (Thermo Fisher Scientific), supplemented with 10% FBS, 100 U/mL penicillin, 100 μg/mL streptomycin. Myofibers were maintained in culture at 37°C with 5% CO_2.

METHOD DETAILS

Plasmids and *in vitro* transfection

Plasmids encoding mitochondria targeted aequorin (mitAEQ) (Rizzuto et al., 1992), cytosolic aequorin (cytAEQ) (Brini et al., 1995), and the mitochondria targeted GCaMP6f probe (4mtGCaMP6f) (Tosatto et al., 2016) were previously described. pC1-HyPer-Red was a gift from Vsevolod Belousov (Addgene plasmid # 48249; http://addgene.org/48249; RRID:Addgene_48249). pLPCX mito Grx1-roGFP2 was a gift from Tobias Dick (Addgene plasmid # 64977; http://addgene.org/64977; RRID:Addgene_64977). Plasmid encoding mit-Hyper Red was previously described (Ermakova et al., 2014).

HeLa cells were transfected with a standard Ca^{2+} phosphate procedure as already described (De Stefani et al., 2011). MDA-MB-231 were transfected with LipofectamineTM 2000 transfection reagent (Invitrogen).

Construction of adenoviral vectors for 4mtGCamp6f probe

The adenovirus expressing 4mtGCaMP6f was generated using the AdEasy strategy (Agilent). 4mtGCaMP6f (Tosatto et al., 2016) was subcloned in the pShuttle-CMV vector (Agilent) from pcDNA3.1-4mtGCaMP (Tosatto et al., 2016) using the following primers:

fw: 5′- AATTTAGATCTCCAAGCTGGCTAGCATGTCC-3′
rv: 5′- AAATTGCGGCCGCTCACTTCGCTGTCATCATTT -3′

The PCR fragment was cloned into BglII and NotI sites in pShuttle-CMV (pShuttle-CMV was a gift from Bert Vogelstein (Addgene plasmid # 16403)). Subsequent steps were performed according to the manufacturer's instructions (Agilent).

C2C12 Adenoviral infection

C2C12 myoblasts were seeded in a 6- well plate. 24 h later cells were infected with Ad-mCherry-U6-scramble-shRNA (Ad-shscr), or Ad-mCherry-U6-m-MCU-shRNA (Ad-shMCU) (8,6 × 10^7 PFU, Vector Biolabs). 48 h later growth medium was replaced with 2% HS-containing medium to induce myotube formation. MCU silencing was monitored by western blotting 9 days after infection.

In vivo DNA transfection of mouse skeletal muscles and myofiber isolation

Hyaluronidase solution (2 mg/ml) (Sigma-Aldrich) was injected in the hind limb footpad of anesthetized animals. 30 min later, 20 μg of plasmid DNA in 20 μl of 0.9% NaCl solution was injected. One gold-plated acupuncture needle was placed under the skin at heel, and a second one at the base of the toes, oriented parallel to each other and perpendicular to the longitudinal axis of the foot and connected to a BTX Electroporation System (Harvard apparatus). 20 pulses, 20 ms each, 1 s of interval were applied to yield an electric field of 100 V. FDB fibers were isolated 7 days after *in vivo* transfection. Muscles were digested in collagenase A (4 mg/ml) (Roche) dissolved in Tyrode's salt solution (pH 7.4) (Sigma-Aldrich) containing 10% FBS. Single fibers were isolated, plated on laminin-coated glass coverslips and cultured for 24 h before performing experiments.

Drugs

Amorolfine hydrochloride (IUPAC name (2R,6S)-2,6-dimethyl-4-[2-methyl-3-[4-(2-methylbutan-2-yl)phenyl]propyl]morpholine;hydrochloride);

Benzethonium chloride (IUPAC name benzyl-dimethyl-[2-[2-[4-(2,4,4-trimethylpentan-2-yl)phenoxy]ethoxy]ethyl]azanium;chloride);

Duloxetine hydrochloride (IUPAC name (3S)-N-methyl-3-naphthalen-1-yloxy-3-thiophen-2-ylpropan-1-amine;hydrochloride); were purchased from Sigma Aldrich (cat. Y0001795, B8879, PHR1865 respectively).

High-throughput Ca^{2+} measurements and data analysis

The Pharmakon-1600 collection was purchased from Microsource Discovery Systems Inc. Three replicate measurements with all compounds were performed using both the cytosolic and mitochondrial aequorin probes. The 20 (96 well) compound plates were measured on 60 (cyt) and 60 (mit) plates. Each plate included 12 dimethyl sulfoxide (DMSO) controls. In the collection, most compounds were 10mM, except some of them, as detailed in Table S1. For calcium measurements, all compounds were diluted 1000 fold.

HeLa cells were transfected with mitAEQ or cytAEQ plasmids (Tosatto et al., 2017) in 24-well plates and then split in 96-well plates. 24 h later, cells were incubated with 5 μM coelenterazine for 1 h to reconstitute the AEQ probes. Coelenterazine solution was removed and cells were treated for 30 min either with the drugs (1:1000 dilution) or DMSO (0.1% v/v) in a modified Krebs-Ringer buffer (KRB) (125 mM NaCl, 5 mM KCl, 1 mM Na_3PO_4, 1 mM $MgSO_4$, 5.5 mM glucose, 20 mM HEPES [pH 7.4]). Ca^{2+} measurements were performed in the EnVision plate reader equipped with a two injectors unit (PerkinElmer). Histamine (100 μM) was injected to trigger Ca^{2+} transients, and then a hypotonic, Ca^{2+}-rich, digitonin-containing solution (100 μM digitonin, 10 mM $CaCl_2$) was added to discharge the remaining aequorin pool. Luminescence from each well was measured for 1 min. The light signal was collected and calibrated into $[Ca^{2+}]$ values by an algorithm based on the Ca^{2+} response curve of aequorin at physiological conditions of pH, $[Mg^{2+}]$ and ionic strength, as previously described (Feno et al., 2019) .

The peak values were analyzed using the cellHTS2 R package (Bioconductor: 10.18129/B9.bioc.cellHTS2). Multiplicative per-plate normalization method was applied, using the median of the negative controls. The means of the replicates were used to calculate Z-scores for each compound (Figure 1; Table S1).

Small-scale Ca^{2+} measurements

Measurements in cell lines with Aequorin probes

For measurements of $[Ca^{2+}]_{cyt}$ and $[Ca^{2+}]_{mit}$, HeLa and MDA-MB-231 cells were grown on 13-mm round glass coverslips and transfected as previously described (De Stefani et al., 2011). 48 h later, cells were incubated with 5 μM coelenterazine for 1 h in KRB at 37°C supplemented with 1 mM $CaCl_2$. In experiments with intact cells, those were transferred to the perfusion chamber where Ca^{2+} transients were evoked by Histamine (100 μM) or ATP (100 μM) (Sigma) as indicated. 30 s before agonist addition drugs dissolved in DMSO 0.1% (v/v) were added and maintained during stimulation. In some experiments drugs were added at different time points as specified. At the end of the experiment cells were lysed with 100 μM digitonin in a hypotonic Ca^{2+}-rich solution (10 mM $CaCl_2$ in H_2O), thus discharging the remaining aequorin pool. The light signal was collected and calibrated into $[Ca^{2+}]$ values by an algorithm based on the Ca^{2+} response curve of aequorin at physiological conditions of pH, $[Mg^{2+}]$ and ionic strength, as previously described (Tosatto et al., 2017).

In the experiments with permeabilized cells, a buffer mimicking the cytosolic ionic composition (IB) was employed: 130 mM KCl, 10 mM NaCl, 2 mM K_2HPO_4, 5 mM succinic acid, 5 mM malic acid, 1 mM $MgCl_2$, 20 mM HEPES, and 1 mM pyruvate (pH 7) at 37°C. IB was supplemented with either 100 mM EGTA (IB/EGTA) or a 2 mM EGTA-buffered $[Ca^{2+}]$ of the indicated concentration (IB/Ca^{2+}). HeLa cells were permeabilized by a 1 min perfusion with 100 μM digitonin (added to IB/EGTA) during luminescence measurements. Drugs or DMSO (0.1% v/v) were added to the different perfusion buffers during the entire duration of the experiment. Mitochondrial Ca^{2+} uptake speed was calculated as the first derivative by using the slope Excel function and smoothed for three time points. The higher value reached during Ca^{2+} addition represents the maximal Ca^{2+} uptake speed.

Mitochondrial Ca^{2+} measurements in C2C12 myoblasts

C2C12 myoblasts were grown on 24 mm coverslips. 24 h later they were infected with adenoviral particles expressing 4mtGCaMP6f (Ad-4mtGCaMP6f). 24 h after infection, amorolfine or DMSO (0.1% v/v) in $CaCl_2$ (1mM)-containing KRB was added immediately before the recording. After 30 s of acquisition, cells were treated with carbachol (100 μM) and images were recorded for other 50 s.

Mitochondrial Ca^{2+} measurements in adult isolated myofibers

FDB muscles of 2-4 month-old male mice were electroporated with plasmids encoding 4mtGCaMP6f. 7 days later myofibers were isolated as described above. 24 h after myofiber isolation, real-time imaging was performed. During the experiments, myofibers were maintained in KRB at RT, in the presence of 75 μM N-benzyl-P-toluenesulfonamide (BTS, Tocris) to avoid fiber contraction. 3 min after the addition of amorolfine (10 μM), 40 mM caffeine (Sigma-Aldrich) was added to elicit Ca^{2+} release from intracellular stores. Experiments were performed on a Zeiss Axiovert 200 microscope equipped with a × 40/1.3 N.A. PlanFluor objective. Excitation was performed with a DeltaRAM V high-speed monochromator (Photon Technology International) equipped with a 75 W xenon arc lamp. Images were captured with a high sensitivity Evolve 512 Delta EMCCD (Photometrics). The system is controlled by MetaMorph 7.5 (Molecular Devices) and was assembled by Crisel Instruments. 4mt GCaMP6f was excited every second at 490/20 and 403/20 nm band-pass excitation filters and images were collected through a dual band emission filter (520/40 and 630/60). Exposure time was set to 50 ms. Acquisition was performed at binning 1 with 200 of EM gain. Changes in Ca^{2+} levels (490/403 nm fluorescence ratio) were expressed as R/R_0, where R is the ratio at time t and R_0 is the ratio at the beginning of the experiment. Mitochondrial Ca^{2+} peak was expressed as $(R\text{-}R_0)/R_0$ and normalized for the control value. Analysis was performed with the Fiji distribution of ImageJ (Schindelin et al., 2012). Images were background corrected frame by frame by subtracting the mean pixel value of a cell-free region of interest.

Cytosolic Ca^{2+} measurements with FURA-AM

C2C12 myoblasts, grown on 24 mm coverslips, were loaded with 5 μM FURA-2/AM (cell-permeant acetoxymethyl ester) in (1 mM) $CaCl_2$ -containing KRB supplemented with 0.05% Pluronic F-127 at 37°C for 30 min. Then they were washed twice with (1 mM) $CaCl_2$ -containing KRB and incubated with amorolfine or DMSO (0.1% v/v) immediately before recording. After 30 s of acquisition cell were treated with carbachol (100 μM) and the images were recorded for other 50 s.

Cytosolic Ca^{2+} measurements in adult isolated myofibers

Myofibers of 2-4 month-old male mice were isolated as described above. 24 h later myofibers were loaded with FURA-2/AM (5 μM) in (1 mM) $CaCl_2$ -containing KRB supplemented with 0.05% Pluronic F-127 at 37°C for 30 min and real-time imaging was performed. During the experiments, myofibers were maintained in KRB at RT, in the presence of 75 μM BTS (Tocris) to avoid fiber contraction. 3 min after the addition of amorolfine (10 μM), 40 mM caffeine (Sigma-Aldrich) was added to elicit Ca^{2+} release from intracellular stores. Images were taken by using a Zeiss Axiovert 200 microscope equipped with a 40 × /1.4 N.A. PlanFluar objective. Excitation was performed with a DeltaRAM V highspeed monochromator (Photon Technology International) equipped with a 75 W xenon arc lamp. Images were captured with a high-sensitivity Evolve 512 Delta EMCCD (Photometrics). The system is controlled by MetaMorph 7.5 (Molecular Devices) and was assembled by Crisel Instruments. Cells were alternatively illuminated at 340 and 380 nm, and fluorescence was collected through a 515/30-nm band-pass filter (Semrock). Exposure time was set to 200 ms at 340 nm and to 400 ms at 380 nm, in order to account for the low quantum yield at the latter wavelength. The image analysis software Fiji was used to correct images the same way as it was described above. Data are presented as the mean of the averaged ratio of all time points.

Mitochondrial Ca^{2+} uptake measurements in permeabilized HeLa cells by Calcium Green-5N fluorescence

HeLa cells were washed with phosphate-buffered saline (PBS) and resuspended with KCl buffer (125 mM KCl, 5 mM NaCl, 2 mM K_2HPO_4, 1 mM $MgCl_2$, 20mM HEPES, pH 7.2) supplemented with 5mM glutamate and malate, 100 μM digitonin, 10 μM EGTA, 1 μM Thapsigargin and 0.5 μM Calcium Green-5N (Invitrogen). A first bolus of $CaCl_2$ (15 μM) was added causing a steep increase in Calcium Green fluorescence. When Calcium Green fluorescence returned to basal levels, DMSO (0.1% v/v), amorolfine (10 μM) or benzethonium (10 μM) were added. Three minutes later, a second bolus of $CaCl_2$ (15 μM) was added. For each sample, the ratio of the two rates of mitochondrial Ca^{2+} uptake after and before drug addition was calculated. Values were reported as percentage of vehicle ratio.

EC_{50} calculation

EC_{50} of amorolfine

HeLa cells were transfected with mitAEQ plasmid as previously described (De Stefani et al., 2011). 48 h later cells were treated with amorolfine (0.5 μM, 1 μM, 10 μM, 50 μM, 100 μM, 300 μM, 500 μM) or DMSO (0.1% v/v) before (30 s) and during stimulation. Ca^{2+} transients were evoked by Histamine (100 μM). C2C12 myoblasts were infected with Ad-4mtGCaMP6f and treated with amorolfine (0.005 μM, 0.010 μM, 0.025 μM, 0.050 μM, 0.1 μM and 0.5 μM) or DMSO (0.1% v/v) immediately before measurements. After 30 s of acquisition, cells were treated with carbachol (100 μM) and images were recorded for additional 50 s as described above.

EC_{50} of benzethonium

HeLa cells were transfected with mitAEQ plasmid as previously described (De Stefani et al., 2011). 48 h later cells treated with benzethonium (0.1 μM, 1 μM, 10 μM, 25 μM, 40 μM, 50 μM, 60 μM, 100 μM) or DMSO (0.1% v/v) for 1 h. Cells were then kept in benzethonium (0.1 μM, 1 μM, 10 μM, 25 μM, 40 μM, 50 μM, 60 μM, 100 μM) or DMSO (0.1% v/v) before (30 s) and during stimulation. Ca^{2+} transients were evoked by Histamine (100 μM). MDA-MB-231 cells were transfected with mitAEQ and incubated with benzethonium (0.1 μM, 0.125 μM, 0.25 μM, 0.5 μM, 0.75 μM, 1 μM) or DMSO (0.1%v/v) for 48 h. Mitochondrial Ca^{2+} transients were evoked by ATP (100 μM) as described above.

In all cases mitochondrial [Ca^{2+}] peaks were normalized to those of the corresponding DMSO controls, transformed into logarithmic values and processed by the non-linear regression function of Graphpad Prism 8.0.2 (263), based on the 4-parameter logistic model. EC_{50} has been determined by calculating the inflection point of each curve.

Oxygen consumption rate (OCR) measurements

OCR in adult isolated myofibers

FDB myofibers were isolated, plated on laminin-coated XF24 microplate wells and cultured in DMEM (Sigma Aldrich), supplemented with 1 mM Na^+ Pyruvate, 5 mM glucose, 33 mM NaCl, 15 mg phenol red, 25 mM HEPES, and 1 mM of L-Glutamine. Fibers were maintained for 2 h in culture at 37°C in 5% CO_2. The rate of oxygen consumption was assessed in realtime with the XF24 Extracellular Flux Analyzer (Agilent). A titration with the uncoupler CCCP was performed in order to utilize the CCCP concentration (1 μM) that maximally increases OCR. The results were normalized for the fluorescence of Calcein (Sigma-Aldrich). Fibers were loaded with 2 μM Calcein for 30 min. Fluorescence was measured using a Perkin Elmer EnVision plate reader in well scan mode using 480/20 nm filter for excitation and 535/20 nm filter for emission.

OCR in MDA-MB-231 cells

Cells were plated in XF24-well cell culture microplates (Agilent). 24 h later they were treated with benzethonium (0.5 μM or 1 μM) or DMSO (0.1% v/v) in serum-free medium. 48 h later cell medium was substituted with DMEM (Sigma Aldrich), supplemented with 1 mM Na^+ Pyruvate, 5 mM glucose, 33 mM NaCl, 25 mM HEPES, and 1 mM of L-Glutamine, in the presence of benzethonium

(0.5 μM or 1 μM) or DMSO (0.1% v/v). The rate of oxygen consumption was assessed in realtime with the XF24 Extracellular Flux Analyzer (Agilent). A titration was performed in order to utilize the carbonyl cyanide-p-trifluoromethoxyphenylhydrazone (CCCP) concentration (0.5 μM) that maximally increases OCR. The results were normalized for the protein content.

ROS production measurement

Superoxide anion

MDA-MB-231 cells were treated with benzethonium (0.5 μM or 1 μM) or DMSO (0.1% v/v). 48 h later cells were loaded with 5 μM MitoSOX TM Red reagent (Life Technologies) for 15 min at 37°C. MitoSOX TM Red excitation was performed at ~510 nm, and emission was collected at 580 nm. Maximal ROS production was induced with 2 μM Antimycin-A (Sigma-Aldrich). Images were taken every second with a fixed 500 ms exposure time.

Mitochondrial and cytosolic H_2O_2

MDA-MB-231 cells were transfected with plasmids encoding mit-Hyper Red or Hyper Red probe respectively and treated with benzethonium (0.5 μM or 1 μM) or DMSO (0.1% v/v) for 48 h. mit-Hyper Red and Hyper Red excitation was performed at 560 nm, and emission was collected at 605 nm. Maximal ROS production was induced with 200 μM H_20_2 (Sigma-Aldrich). Images were taken every second with a fixed 500 ms exposure time.

Mitochondrial GSSG/GSH

MDA-MB-231 cells were transfected with a plasmid encoding the ratiometric pLPCXmitGrx1-roGFP2 probe and treated with benzethonium (0.5 μM or 1 μM) or DMSO (0.1% v/v) for 48 h. pLPCXmitGrx1-roGFP2 excitation was performed at 405 nm and 488 nm and emission was collected at 530 nm. Maximal ROS production was induced with 200 μM H_20_2 (Sigma-Aldrich). Images were taken every second with a fixed 500 ms exposure time.

In all cases images were taken on an inverted microscope (Zeiss Axiovert 200) equipped with a PlanFluar 60 × /1.4 NA objective, a Photometrics Evolve Delta EMCCD, and a 75 W Xenon arc lamp coupled to a monochromator (PTI Deltaram V). The system was assembled by Crisel Instruments. Data were analyzed by ImageJ software.

Mitochondrial membrane potential ($\Delta\Psi_m$) measurements

HeLa and MDA-MB-231 cells were cultured on coverslips, incubated with 20 nM tetramethyl rhodamine methyl ester dye (TMRM) (Life Technologies) in KRB for 20 min at 37°C. Drugs were either added before experiments at different time points or 2 min after the first acquisition. The probe was excited at 560 nm, and the emission light was recorded in the 590–650 nm range; 10 μM CCCP was added at the end of the experiment to completely collapse the $\Delta\Psi_m$. Data are expressed as difference of TMRM fluorescence before and after CCCP depolarization.

C2C12 morphological analysis

C2C12 myoblasts were cultured in DMEM supplemented with 10% FBS. When cells reached 90% confluence, medium was replaced with DMEM containing 2%-heat inactivated horse serum in the presence of amorolfine or DMSO (0.1% v/v). Cells were maintained in these conditions for three or seven days (in the latter case medium was replaced every three days). In MCU silencing experiments, the seeded myoblasts were infected with Ad-mCherry-U6-scramble-shRNA (Ad-shscr) or Ad-mCherry-U6-m-MCU-shRNA (Ad-shMCU) ($8{,}6 \times 10^7$ PFU, Vector Biolabs). 48 h later cells were incubated with amorolfine (0.5 μM) or DMSO (0.1% v/v) for seven days. At the end of the experiment, myotube images were taken and myotube width and length were measured by means of ImageJ software.

Myofiber size analysis

Amorolfine (1 mM) was injected in TA muscles of mice for 10 days every 48 h. In parallel, DMSO (10% v/v) was injected in muscles of control animals. For fiber size measurements, 20 μm-thick cryosections were fixed in 4% formaldehyde for 20 min, quenched with 50 mM NH_4Cl in PBS and blocked in PBS containing 0.5% bovine serum albumin (BSA) for 20 min. Sections were then incubated with primary anti-Laminin antibody (Sigma-Aldrich) for 1 h at 37°C to label the sarcolemma and washed 3 times in PBS. Alexa Fluor 488-conjugated secondary antibody (Thermo Fisher Scientific) was used. Fiber size measurements were performed with the Fiji image processing software.

Cell viability assays

MTS assay

HeLa cells grown in a 96-well plate were treated for 24 h with amorolfine (10 μM) or DMSO (0.1% v/v). C2C12 myoblasts grown in a 96-well plate were treated with amorolfine (0.1 μM, 0.5 μM, 1 μM, 10 μM) or DMSO (0.1% v/v) for 3 and 5 days. At the end of the treatment, cells were incubated with [3-(4,5-dimethylthiazol-2-yl)-5-(3-carboxymethoxyphenyl)-2-(4-sulfophenyl)-2H-tetrazolium] (MTS) (Promega) for 1 h. During incubation, the metabolically active cells convert MTS into its reduced form formazan that is released in the extracellular medium and that has a maximal absorbance at 490nm. Thus, cell media were collected and absorbance at 490nm was measured by means of an Infinite plate reader 200 pro (TECAN). The percentage of cell survival was obtained by normalizing the absorbance of medium of amorolfine-treated cells to that of control medium.

Fluorescence activated cell sorting (FACS) analysis

MDA-MB-231 cells were incubated with benzethonium (1 μM) for 48 h. In some experiments, ceramide (40 μM) was added for the last 2 h before analysis. Cells were collected and treated with Annexin V APC and with propidium iodide (eBioscience Annexin V Apoptosis detection kit APC, Invitrogen). Cell populations were analyzed by FACS (FACS Canto II, BD BioSciences). Data were processed using the BD Vista software.

Cell proliferation assay

MDA-MB-231 cells and MCU$^{-/-}$ MDA-MB-231 clones were treated with benzethonium or DMSO (0.1% v/v). Cell number was counted every 24 h for two days. Results are expressed as ratio R/R0 where R is the number of cells at the time (t) and R0 is the number of cells at the time of incubation with benzethonium.

Clonogenic assay

To evaluate the clonogenic potential, MDA-MB-231 cells were seeded (10^3 cells for each well). 24 h later benzethonium or DMSO (0.1% v/v) were added. 7 days later colonies containing $\geq$ 30 cells were counted.

Migration assay

MDA-MB-231 cells and MCU$^{-/-}$ MDA-MB-231 clones were seeded at low confluency (30%) in 6-well plates. 24 h later they were treated with benzethonium (0.5 μM or 1 μM) or DMSO (0.1% v/v) in serum-free medium. At the same time a linear scratch was obtained on cell monolayers through a vertically held P200 tip. Images were taken at the indicated time points. ''TScratch'' software (https://cse-lab.ethz.ch/software/) was used for automated image analysis.

RNA extraction, reverse transcription, and quantitative real time PCR

RNA was extracted using the SV Total RNA Isolation Kit (Promega) following manufacturer's instructions. Complementary DNA was generated with a cDNA synthesis kit (SuperScript II, Invitrogen) and analyzed by real-time PCR (Applied Byosistem). GAPDH was used as housekeeping gene. The following primers were used:

MyoD: fw 5′-CTCTGATGGCATGATGGATT-3′; rv 5′-GTGGAGATGCGCTCCACTAT-3′
Myf5: fw 5′-GAGCTGCTGAGGGAACAGGTGGAGA-3′; rv, 5′-GTTCTTTCGGGACCAGACAGGGCTG-3′
GAPDH: fw 5′-CACCATCTTCCAGGAGCGAG-3′; rv, 5′-CCTTCTCCATGGTGGTGAAGAC-3′

Western blotting and antibodies

Myotubes were lysed with RIPA buffer [Tris-HCl pH 6.8 50 mM, NaCl 150 mM, Triton 1% (v/v), sodium deoxycholate 0.5% (v/v), SDS 0.1% (v/v)] containing protease and phosphatase inhibitor cocktails (Roche). Lysates were subjected to SDS-PAGE and blotted onto nitrocellulose membranes (0.45 μm pore size, Biorad). Membranes were incubated for 1 h at RT with a blocking solution followed by incubation (overnight, 4°C) with one of the following primary antibodies: anti-MCU (Sigma cat. no. HPA016480; 1:1000); anti actin (Santa Cruz Biotechnology cat. no. SC56459; 1:5000). Horseradish peroxidase-conjugated anti-rabbit-IgG, or anti-mouse-IgG secondary Ab (Santa Cruz Biotechnology cat. no. sc-2004/2005) were used. Immunoreactive bands were visualized and digitalized by means of a digital Uvitec Image Station, using an enhanced chemiluminescence reagent kit (Millipore). Immunoreactive bands were analyzed by ImageJ software.

QUANTIFICATION AND STATISTICAL ANALYSIS

Statistics are reported in the figure legends and in Table S2. All results are representative of at least 3 independent experiments unless otherwise specified and are presented as mean ± SD. Significance was calculated by Student's two-tailed non-paired t test, ANOVA (one-way or two-way) or by Mann-Whitney Rank Sum Test. All statistical tests were run with SigmaPLot. P values < 0.05 were considered statistically significant and marked with asterisks (*$p < 0.05$; **$p < 0.01$; ***$p < 0.001$).